

A study of the passive gait of a compass-like biped robot: symmetry and chaos

Ambarish Goswami[†], Benoit Thuilot[‡]*, Bernard Espiau[†]

[†]INRIA Rhône-Alpes
655 avenue de l'Europe, ZIRST
38330 Montbonnot Saint Martin, France

[‡]LASMEA - Groupe GRAVIR
Université Blaise Pascal
Campus universitaire des Cezeaux
63177 Aubiere Cedex, France

Communicating Author E-mail: Ambarish.Goswami@inrialpes.fr

International Journal of Robotics Research
(in press)

Abstract

The focus of this work is a systematic study of the passive gait of a compass-like planar biped robot on inclined slopes. The robot is kinematically equivalent to a double pendulum, possessing two kneeless legs with point masses and a third point mass at the "hip" joint. Three parameters, namely the ground slope angle and the normalized mass and length of the robot describe its gait. We show that in response to a continuous change in any one of its parameters the symmetric and steady stable gait of the unpowered robot gradually evolves through a regime of bifurcations characterized by progressively complicated asymmetric gaits eventually arriving at an apparently chaotic gait where no two steps are identical. The robot can maintain this gait indefinitely.

A necessary (but not sufficient) condition for the stability of such gaits is the contraction of the "phase fluid" volume. For this frictionless robot the volume contraction, which we compute, is caused by the dissipative effects of the ground impact model. In the chaotic regime the fractal dimension of the robot's strange attractor (2.07) compared to its state-space dimension (4) also reveals strong contraction.

We present a novel graphical technique based on the first return map that compactly captures the entire evolution of the gait, from symmetry to chaos. Additional passive dissipative elements in the robot joint result in a significant improvement in the stability and the versatility of the gait and provides a rich repertoire for simple control laws.

Keywords: biped robot, compass gait, passive gait, phase diagram, Poincaré map, bifurcation, chaotic behavior, dissipative elements

*This work was done while Benoit Thuilot was with INRIA Rhône-Alpes.

1 Motivation

Biped robots and other legged robots are potentially better suited than wheeled vehicles to the maintenance of hazardous environments (nuclear and chemical reactors), exploration of unstructured and unpaved terrains (ocean floors, polar regions, lunar and Martian surfaces), deep-forest logging, fruit harvesting etc. At present, one of the main obstacles to a wider application of legged robots is their lack of energy efficiency. In comparison, their biological analogues demonstrate impressive energy economy during normal walking gait. In fact, EMG studies have shown [32][27] relative muscle inactivity during the swing phase of human walk makes it almost passive. This illustrates the superiority of the biological control strategy which functions in harmony with the natural inertial dynamics of the body in the gravitational field.

The long-term motivation behind the current study is to formulate a simple biologically-inspired active control law for a 17-dof biped robot [5] being built in Project BIP coordinated by the INRIA laboratory in Grenoble, France. The control of such a highly nonlinear dynamic system coupled with the well-known stability issues common to all bipeds represents a major challenge. Experience shows that control strategies unconcerned with the system dynamics fail to take advantage of the benevolent dynamics inherent in the controlled system and risks being a control overkill. In order to gain a better understanding of the dynamics of biped locomotion we find it instructive to first explore the behavior of a simple walker model.

Physical models[26][4] and theoretical and simulation results[9][11] have demonstrated the fact that even passive biped robots with simple kinematics can successfully walk down an inclined slope in a steady gait. The motive power of such robots comes from the conversion of the robot's gravitational potential energy as it descends down the slope. A delicate balance between the kinetic energy available from the conversion of potential energy and that absorbed due to ground impact assures the maintenance of the steady gait. The particular gait adopted by the robot depends on the ground slope as well as its geometric and inertial parameters.

The existence of natural locomotion regimes in such simple machines suggests at the possibility that an attentive but minimal control system based around a tuned dynamic system might represent the most judicious choice for controlling biped robots in complex environments.

What is compass-gait? The biped robot model studied in this paper is the so-called compass-gait model. The gait is so named since the locomotion produced with this model is analogous to the movement of a pair of compasses or dividers. The Cartesian hip trajectory consists of a series of circular arcs centered around the point of contact of the support leg with the ground and having a radius equal to the leg length. A particularly useful analysis of the human gait[32] decomposes the entire gait mechanism into six elementary "determinants," each involving a single degree-of-freedom (dof) in one of the joints. Compass gait is the first determinant of gait and it is the simplest kinematics that may exhibit a bipedal walking gait. Despite its simplicity, on a descending slope a passive compass gait robot may exhibit "dynamic gait," [26] which means that its center of mass is not constrained to stay atop its foot support point. This feature is normally associated with the anthropomorphic gait and attributed to a superior control performance.

The robot model, discussed in greater detail in Section 2.1, consists of two kneeless legs each having a point mass, and a third point mass coincident with the hip joint. The Acrobot[2][34] and the Pendubot[3] are also based on the same double pendulum kinematics although they do not possess the hip mass. [19] and [38] present studies of other kneeless bipeds with an additional body mass connected to the hip through a pelvic joint. In [19] particular attention was paid to the effect of robot's impact with the ground and the impact conditions were justifiably considered as an integral part of the governing equations. Bipeds with very simple dynamics were also constructed [21][13][7]. These models have telescopically retractable legs. The former of this is a 3-dof model with independently adjustable leg lengths whereas in the latter two the sum of the leg lengths was mechanically constrained to be constant. Each of the robot models mentioned in this paragraph has some form of actuation.

The literature on *passive* bipedal walk is relatively limited. Inspired by the research[28] on ballistic walking, [26] studied and built passive dynamic robots with and without knees. The physical models of these robots demonstrate the remarkable elegance and simplicity of unpowered walking on inclined slopes. A linearized dynamic model of the robot was considered for the analysis of the gait. The effect of variation of few design parameters, including the height of leg center of mass, hip mass fraction and the leg length mismatch, on the walking performance was studied. A leg length mismatch caused, expectedly, a 2-period gait. Curiously, for a larger mismatch a four periodic gait was found.

More recently, a systematic study of the full non-linear equations of a simple compass-like passive biped robot was considered in [10][11][12][35]. [10] associated the steady motion of the robot with a phase plane limit cycle (following [21][19]), and was the first to report the occurrence of a period-doubling bifurcation for this robot. Precursors to the current paper, [12] and [35] studied the effect of a parameter change on the gait of the robot. In response to a parameter change the robot gait was found to exhibit period doubling cascade finally leading to a chaotic motion. The fractal dimension of the chaotic attractor was measured.

In another recent work, [9] considers an even simpler biped model, the “point-foot walker,” which is also based on the same double pendulum kinematics. As explained later, their model can be obtained as a simpler special case of the compass-gait model considered in the current paper. The significant reduction in the complexity of the model permits an analytical computation initial conditions and the stability estimates of 1-periodic gaits. The authors independently found the occurrence of period doubling and was the first to find a chaotic gait in this model. [4] developed a simple 3D passive dynamic Tinkertoy¹ device that walks.

Summary of results This paper presents a systematic study of the passive bipedal gait of a compass-like robot in response to continuous changes in its motion-determining parameters. Three parameters, namely the ground slope angle and the normalized mass and length describe the robot’s dynamic behavior.

As a first guess for the initial states of the robot that will lead it to a stable limit cycle gait, we use the prediction based on the linear model. Once a phase space limit cycle is found we can numerically prove its stability by calculating the Jacobian matrix of the Poincaré map of the limit cycle, as is done for “stride function”[26]. Contraction of phase-space volumes is known as a necessary (but not sufficient) condition for the asymptotic stability of dynamic systems. For our otherwise frictionless robot, the volume contraction is caused by the foot-ground collisions. We quantify the dissipative effects of the ground impact model by measuring the “phase fluid” volume contraction.

A small change in a parameter normally results in small changes in the robot’s gait while its global qualitative behavior remains intact. We find that both the step period and the step length of the robot increase with an increase in any of the three parameters. The robot’s translational velocity, however, increases with slope and normalized mass but decreases with the normalized length. Also most of the quantities describing the robot gait are monotonic functions of the three parameters.

However, there are situations when as one of the parameters exceeds a certain limiting value, a so-called *structural instability* sets in. This is manifested by a large-scale qualitative change in the gait. These structural instabilities are associated with period-doubling bifurcations in the solution of the robot’s governing equations. As the parameter continues to change the system may undergo a cascade of repeated bifurcations, and may, in the long run, exhibit chaotic behavior. Many of the tell-tale signs of chaos such as a “broad-band frequency,” similar but non-identical cycles and a densely packed attractor are all exhibited by these latter gaits.

We present a novel graphical technique based on the first return map that compactly captures the entire evolution of the gait, from symmetry to chaos. The fractal dimension of the attractor is computed to be 2.07. For a system with a 4-dimensional state-space, this indicates strong phase-space volume contraction.

Additional passive dissipative elements in the robot joint result in a significant improvement in the stability and versatility of the gait and provide a rich repertoire for simple control laws.

2 Modeling

2.1 Robot model and modeling assumptions

Fig. 1 shows a sketch of a compass-like biped robot. The details of the model and the underlying assumptions are listed below:

- Mass: concentrated at 3 points:
 - mass m_H at the hip,
 - masses m on each leg, located at distances a and b from respectively the leg tip and the hip.

¹Registered Trademark

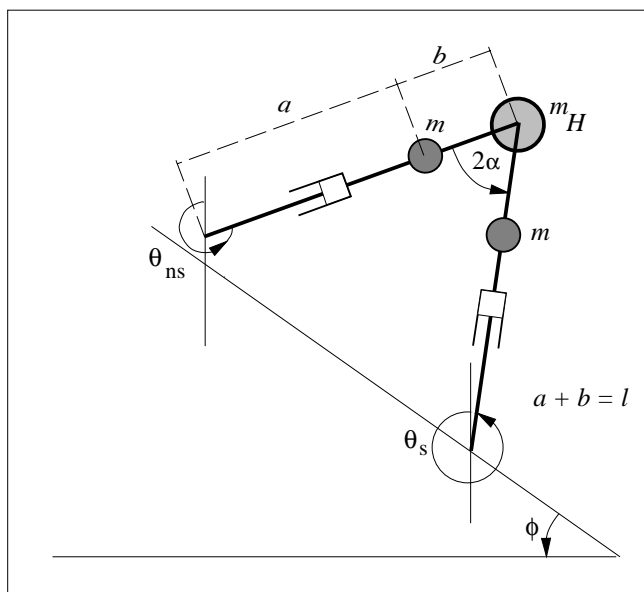


Figure 1: Sketch of a compass-like biped robot on a slope. The robot consists of two kneeless legs each having a point mass, and a third point mass coincides with the hip joint. The prismatic-joint knee shown in the picture is an imaginary concoction meant to avoid the conceptual foot-clearance problem. See Section 2.1 for details.

- The total mass of the robot $m_C = 2m + m_h$ is constant and equal to 20 Kg, whereas the *mass ratio* $\mu = \frac{m_H}{m}$ will be varied from 0.1 to 10 during the simulation trials.
- Leg: the legs are identical. The leg length $l = a + b$ is constant and equal to 1 meter, whereas the *length ratio* $\beta = \frac{b}{a}$ will be varied from 0.1 to 10 during the simulation trials.
 - Actuation: the robot is unactuated.
 - Ground: the robot walks down on a plane surface inclined at a constant angle ϕ with the horizontal.
 - Gait: The motion is constrained in the sagittal plane and consists of the following two stages :
 - *Swing*: during this stage the robot hip pivots around the point of support on the ground of its *support leg*. The other leg, called the *non-support leg* or the *swing leg* swings forward (the compass robot in Fig. 1 is in swing stage).
 - *Transition*: it occurs instantaneously when the swing leg touches the ground and the previous support leg leaves the ground.
 - Ground impact: the impact of the swing leg with the ground is assumed to be slipless plastic. This implies that during the instantaneous transition stage (see for instance [18]):
 - the robot configuration remains unchanged,
 - the angular momentum of the robot about the impacting foot as well as the angular momentum of the pre-impact support leg about the hip are conserved. These conservation laws lead to a discontinuous change in robot velocity.
 - Prismatic-joint knee: This is a purely imaginary concoction meant to address the conceptual problem of foot-clearance common to all kneeless planar bipeds. The prismatic joint is assumed to retract the lower leg to clear the ground. The retraction of the lower leg, which is assumed massless, does not affect the robot dynamics. The swing leg returns to its original length l at transition. Our emphasis here is on the simplicity of the model rather than its physical realizability. Note however that physical models of robots of this type were developed and studied in [13][21].
 - Nominal model: Although we study the passive gait of the robot for a range of parameters specified earlier, certain results in this paper are centered around a nominal robot model which corresponds to $\mu = 2$ and $\beta = 1$. For results involving other models, the parameters of the robot will be specified..

During swing, the robot configuration can be described by $\boldsymbol{\theta} = [\theta_{ns}, \theta_s]^T$ where θ_{ns} and θ_s are the angles made respectively by the non-support (swing) and the support leg with the vertical (counterclockwise positive). The state vector \mathbf{q} associated with the robot is:

$$\mathbf{q} = [\boldsymbol{\theta}, \dot{\boldsymbol{\theta}}]^T = [\theta_{ns}, \theta_s, \dot{\theta}_{ns}, \dot{\theta}_s]^T \quad (1)$$

During transition, since both legs are in contact with the ground, the robot configuration can be completely described by the half inter-leg angle α , or equivalently by the step length L , defined as the distance between robot feet. α and L are related by $L = 2l \sin \alpha$.

Before leaving this section let us provide the definitions of certain terms that we will frequently use in this paper. A gait is **symmetric** if any two consecutive steps are indistinguishable, i.e., all the spatio-temporal variables exactly repeat themselves in each step. When a gait does not possess this property it is said to be **asymmetric**. A gait is **periodic** if all the spatio-temporal variables repeat themselves after every p steps. The integer p is called the **gait period**. For symmetric gaits $p = 1$. In case of a p -periodic gait the **gait cycle** consists of p successive steps. The term **steady gait** is loosely used to mean that the robot can indefinitely continue to walk without falling down. **Step period** is the time to take a **step**, i.e., the time between the take-off of one foot from the ground and its subsequent landing.

As the robot walks, the forward component of velocity of its center of mass changes continuously (as in the human locomotion). Therefore we introduce the term **average speed of progression** of the robot, denoted as v , in order to quantify its forward movement averaged over a cycle. In case of a 2^n -periodic gait, v is a constant. When $n = 0$ (i.e., symmetric gait), v is expressed as $\frac{L}{T}$, with T the step period. For larger values of n , v is the value of $\frac{L_k}{T_k}$ (with k a step counter) averaged over 2^n consecutive steps. For a chaotic gait the average speed of progression can be calculated over a certain number of steps and its exact value will be bounded but changing.

2.2 Governing equations

The governing equations of the robot consist of nonlinear differential equations for the swing stage and algebraic equations for the transition. The equations are well-known (see for example [12]). Here we simply present the symbolic form of the equations expressed in terms of the normalized parameters μ and β . As is true in general, the study of governing equations of the robot in terms of normalized parameters brings in significant advantages. The swing stage equations of the robot, similar to that of a frictionless double pendulum, can be written as:

$$\mathbf{M}(\boldsymbol{\theta})\ddot{\boldsymbol{\theta}} + \mathbf{N}(\boldsymbol{\theta}, \dot{\boldsymbol{\theta}})\dot{\boldsymbol{\theta}} + \frac{1}{a}\mathbf{g}(\boldsymbol{\theta}) = 0 \quad (2)$$

where $\mathbf{M}(\boldsymbol{\theta})$, $\mathbf{N}(\boldsymbol{\theta}, \dot{\boldsymbol{\theta}})$ and $\mathbf{g}(\boldsymbol{\theta})$ depend only on μ and β and not on m , m_H , a and b :

$$\mathbf{M}(\boldsymbol{\theta}) = \begin{pmatrix} \beta^2 & -(1+\beta)\beta \cos 2\alpha \\ -(1+\beta)\beta \cos 2\alpha & (1+\beta)^2(\mu+1)+1 \end{pmatrix} \quad (3)$$

$$\mathbf{N}(\boldsymbol{\theta}, \dot{\boldsymbol{\theta}}) = \begin{pmatrix} 0 & (1+\beta)\beta\dot{\theta}_s \sin(\theta_s - \theta_{ns}) \\ -(1+\beta)\beta\dot{\theta}_{ns} \sin(\theta_s - \theta_{ns}) & 0 \end{pmatrix} \quad (4)$$

$$\mathbf{g}(\boldsymbol{\theta}) = \begin{pmatrix} g\beta \sin \theta_{ns} \\ -((\mu+1)(1+\beta)+1)g \sin \theta_s \end{pmatrix}. \quad (5)$$

The algebraic transition equations relate the robot states just before and just after its collision with the ground. The support and the non-support legs switch during transition. The pre-impact and the post-impact configurations of the robot can be simply related by $\boldsymbol{\theta}^+ = \mathbf{J}\boldsymbol{\theta}^-$ where \mathbf{J} is a 2×2 anti-symmetric matrix with unit elements. The $-$ and the $+$ signs denote the state variables, respectively, before and after the collision. The conservation of angular momentum principle applied to the robot gives us $\mathbf{Q}^-(\alpha)\dot{\boldsymbol{\theta}}^- = \mathbf{Q}^+(\alpha)\dot{\boldsymbol{\theta}}^+$ from which we can write the joint velocity relationship $\dot{\boldsymbol{\theta}}^+ = (\mathbf{Q}^+(\alpha))^{-1}\mathbf{Q}^-(\alpha)\dot{\boldsymbol{\theta}}^- = \mathbf{H}(\alpha)\dot{\boldsymbol{\theta}}^-$ where

$$\mathbf{Q}^-(\alpha) = \begin{pmatrix} -\beta & -\beta + (\mu(1+\beta)^2 + 2(1+\beta))\cos 2\alpha \\ 0 & -\beta \end{pmatrix} \quad (6)$$

$$\mathbf{Q}^+(\alpha) = \begin{pmatrix} \beta(\beta - (1 + \beta)\cos 2\alpha) & (1 + \beta)((1 + \beta) - \beta\cos 2\alpha) \\ \beta^2 & \dots + 1 + \mu(1 + \beta)^2 \\ & -\beta(1 + \beta)\cos 2\alpha \end{pmatrix}. \quad (7)$$

The complete state vector \mathbf{q} before and after impact can thus be written as:

$$\mathbf{q}^+ = \mathbf{W}(\alpha)\mathbf{q}^- \quad (8)$$

with matrix $\mathbf{W}(\alpha) = \begin{pmatrix} \mathbf{J} & 0 \\ 0 & \mathbf{H}(\alpha) \end{pmatrix}$.

It can be shown that the gait characteristics of a robot with arbitrary masses m' and m'_H can always be deduced from those of a robot whose masses are in the same proportion μ [12]. More precisely, the gait characteristics of two different robots, with masses (m', m'_H) and (m, m_H) , such that $\frac{m'}{m} = \frac{m'_H}{m_H} = k_m$ satisfy:

Robot with masses m and m_H	Robot with masses m' and m'_H
$\mathbf{q}, \alpha, L, T, v$	$\mathbf{q}, \alpha, L, T, v$
$E, \Delta E$	$k_m E, k_m \Delta E$

Here E refers to the total mechanical energy of the robot and ΔE is the absorption of energy during the ground impact.

In a similar manner we can show [12] that the gait characteristics of a robot with arbitrary lengths a', b' can always be deduced from those of a robot whose lengths are in the same proportion β . More precisely, the gait characteristics of two different robots, with lengths (a, b) and (a', b') , such that $\frac{a'}{a} = \frac{b'}{b} = k_a$ satisfy:

Robot with lengths a and b	Robot with lengths a' and b'
θ	θ
$\dot{\theta}$	$\frac{1}{\sqrt{k_a}}\dot{\theta}$
α	α
L	$k_a L$
T	$\sqrt{k_a} T$
v	$\sqrt{k_a} v$
E	$k_a E$
ΔE	$k_a \Delta E$

The dynamic model of the robot can therefore be parameterized by μ and β . Note here that the ground slope ϕ , which does not explicitly enter into the governing equations, completes our set of parameters. The effect of these three parameters on the gait characteristics of the passive biped robot is analyzed subsequently.

3 Stable passive gait and limit cycle

Typically, the governing equations for these robots are *hybrid* in the sense that they consist of non-linear differential equations describing the swing stage and algebraic relationships characterizing the switch between two successive swing stages. The ground slope can be imagined to impose an external geometric constraint in the configuration space of the robot, and the switching conditions the result of the robot touching the constraint. The physical model on which the switching conditions are based determines the physical nature of the robot's interaction with the constraint. Changing the ground slope modifies the geometric constraint thereby fundamentally influencing the robot gait. The rich dynamics exhibited by the robot is the result of an interplay between the continuous and the algebraic parts of its governing equations.

3.1 Analytical approach vs simulation

Although the robot has a simple kinematics, the hybrid nature of the governing equations make it impossible to utilize the traditional tools (such as the automatic detection of limit cycles[30]) developed to aid the study of non-linear systems.

There are several approaches that we can adopt in this situation. One approach, as was taken in [26] amongst others, is to linearize the swing stage equations of the robot about an equilibrium state, making it possible to explicitly integrate these equations. Next, the transition equations are concatenated and the conditions for the existence of a periodic solution of this coupled system is found. In order to study the stability of this periodic solution a second linearization about the periodic solution is necessary. The problem with this approach is that the linear solution is valid only within a narrow region around the point of linearization which is typically the stationary vertical configuration of the robot. For any real gait, and especially for higher values of the parameters, we significantly deviate from this point. We will show that this makes the prediction of the long term system behavior impossible.

A second approach, adopted in the recent work of [9], and in a few studies of monopod robots [37] [29] [8], is to simplify the model of the robot so that some analytical insight into the simplified *nonlinear* model is available. For example, the point-foot walker model considered in [9] may be obtained as a special case of our more general model by setting $\frac{m}{m_H} = \frac{1}{\mu} \rightarrow 0$ and $\frac{a}{b} = \frac{1}{\beta} \rightarrow 0$. Because of this simplification the number of robot parameters is reduced from three to one (only the ground slope ϕ) which is useful for graphical visualization and analytical probing. Also it is sometimes possible to obtain an explicit expression for the Poincaré map of the robot. Although an attractive approach, the extension of the results to more complex models is not obvious.

In this study we have thus decided to preserve the full non-linear equations of the robot. The disadvantage in this approach is that our exploration has to rely to a large extent on numerical simulations. However, the computational burden is manageable as the robot model has a relatively small state space dimension and we can focus our study on only one leg of the robot (since the legs are identical, they will have qualitatively identical dynamics). Furthermore, our results can be used to characterize the domain of applicability of linear and simplified non-linear models.

3.2 A typical limit cycle

In order to visualize the entire dynamics of the robot over a gait cycle it is useful to represent the dynamics by means of phase space trajectories. In phase space, steady robot gaits are seen as stable limit cycles and the geometric features of the cycles are characteristic of the particular gait[11][35].

Fig. 2 presents the sketch of a phase space limit cycle of a symmetric gait of the robot on a 3° slope. The sketch is obtained by plotting the angular position and velocity of only one leg. Thus, this is a 2D projection of the limit cycle of the entire robot which is in a 4-dimensional space. For ease of comprehension we have indicated in the figure the time instants of some of the important events during the cycle along with the corresponding stick diagrams of the robot. Let us follow the phase trajectory at the instant marked I corresponding to time $t = 0^+$, when the rear leg just loses contact with the ground (i.e., it becomes the swing leg). The corresponding stick diagram shows a black dot on the front foot to imply ground contact. The phase trajectory evolves in the clockwise sense in this diagram as shown by the arrowheads. While crossing the velocity axis (at a positive velocity), the biped is in the vertical configuration. Instant II corresponds to time $t = T^-$ when the swing leg is about to touch the ground. The impact between the swing foot and the ground occurs at $t = T$. We observe a velocity jump II \rightarrow III due to this impact. The upper half of the cycle (I \rightarrow II) depicts the swing leg suspended as a simple pendulum from a moving point (hip). At instant III ($t = T^+$), the swing leg becomes the support leg and executes the lower half of the phase plane diagram (III \rightarrow IV). This half of the phase portrait corresponds to the motion of the support leg “hinged” at the point of support as an inverted simple pendulum. The velocity jump of the current leg (the non-support leg of instant I) observed between IV and I is due to the impact of the other leg with the ground. The cyclic trajectory is a limit cycle and for stable gaits it attracts and absorbs all nearby trajectories that enter its attraction basin.

3.3 Orbital stability of bipedal gait

Since we often refer to “stability” of the bipedal gait it is helpful to have a precise definition of the term. We consider the notion of *orbital stability* to be the most appropriate in the context

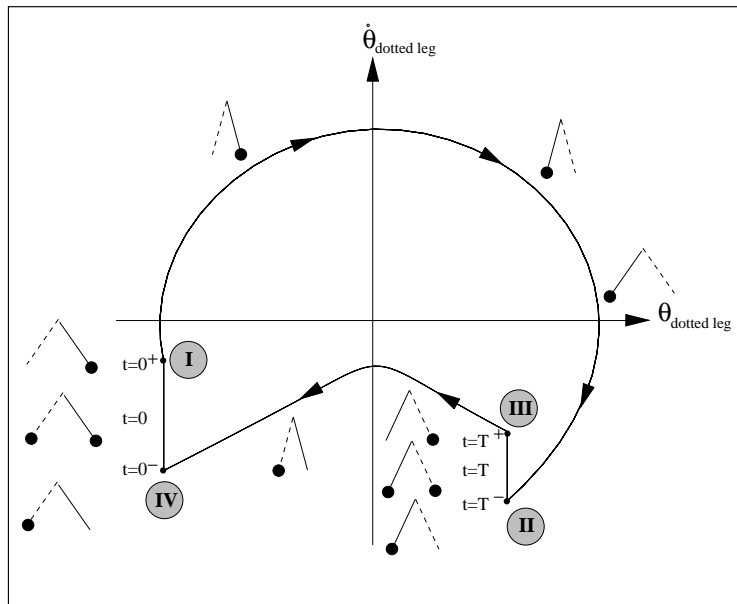


Figure 2: Phase portrait of a symmetric walk. This figure corresponds to only one leg of the biped robot its actual phase space being higher dimensional. One cycle in the figure corresponds to two steps of the robot. In the figure we have indicated some of the time stamps important in the dynamic evolution of the biped. On the outside of the cyclic portrait, the configuration of the biped has been shown with small stick diagrams. In these diagrams, one leg is dotted, the other leg is solid, and a black dot at the foot indicates the supporting leg.

of biped robot dynamics. Qualitatively speaking, a system is orbitally stable if starting from a steady closed phase trajectory, any finite disturbance leads to another nearby trajectory of similar shape [20]. Adapting from [15] we can present this definition in a more mathematical framework. In the phase space of an autonomous system, the phase trajectory C is said to be orbitally stable if *given* $\varepsilon > 0$, *there is* $\delta > 0$ *such that, if* R' *is a representative point (on another trajectory* C') *which is within a distance* δ *of* C *at time* t_0 , *then* R' *remains within a distance* ε *of* C *for* $t \geq 0$. If no such δ exists, C is orbitally unstable. Analogous to the definition of asymptotic stability in the sense of Lyapunov, we may say that *if the trajectory* C *is orbitally stable and, in addition, the distance between* R' *and* C *tends to zero as time goes to infinity, the trajectory* C *is asymptotically orbitally stable.*

The concept of orbital stability is less common in the robotics literature. Orbital stability requires that the trajectories C and C' remain near each other, whereas Lyapunov stability of the solution $\mathbf{q}(t)$ requires that, in addition, the representative points R and R' (on C and C' respectively) should remain close to each other, if they were close to each other initially. Orbital stability does not require that perturbed trajectories “remain in step”.

For a general nonlinear system the analytical demonstration of the existence of a limit cycle, its local orbital stability and the analytical procedure to find it still remain a challenge. However, it is possible to test the local stability of a limit cycle, once it is found. One method to determine the stability of the robot gait is through the numerical computation of its Poincaré map [26][10]. Limit cycles are fixed points of this map, which in the context of biped locomotion, was named the “stride function” [26]. Essentially the procedure consists of injecting small perturbations to the robot states around the limit cycle and calculating the eigenvalues of the sensitivity matrix. For an orbitally stable cycle the eigenvalues lie within the unit circle, i.e., their moduli are strictly less than one.

It has already been demonstrated theoretically [26][10][9] that a passive biped robot walking on inclined slopes can exhibit stable limit cycles. A visual inspection of the gaits of the physical models constructed by [26] appeared to have the quality of stability. Based on the results of their numerical simulations [10] reported that a given robot appears, interestingly, to exhibit one and only one stable gait on a given slope. Depending on the values of the robot parameters ϕ , β , and μ , the gait is symmetric or asymmetric. [9] analytically showed the existence of one stable and one unstable cycle for their point-foot walker walking on small slopes. The current paper focuses on

the stable cycles only, which represent viable passive gaits.

3.4 Orbital stability implies contraction of “phase fluid”

A necessary condition for the existence of stable limit cycle can be obtained by studying the evolution of a small phase space volume element. The complete state of a dynamic system at a certain instant is represented by a point in the phase space of the system. The effect of the perturbations on the system at this state is closely related to the behavior of the so called “phase fluid” [23] around that point. As the dynamic system evolves in course of time, a small volume element around the system state, representing the possible perturbed states, can be imagined to move around it in the phase space. An elegant mathematical treatment culminating in the Liouville’s theorem finds that a small volume element² of the phase space of a Hamiltonian system behaves like an incompressible fluid. Since the Hamiltonian of a frictionless system is constant it can be shown that the divergence of its phase fluid is zero [17]. In other words, the phase space volume element may change its shape depending on the dynamics of the particular system keeping its volume constant all along.

A dissipative system, however, does not obey Liouville’s theorem and for such systems the phase space volume element gradually contracts as it moves. The existence of a stable limit cycle in a dynamical system is associated with such volume contraction. This makes intuitive sense as we know that a volume element in the attraction basin eventually converges on the limit cycle which, being a 1-dimensional entity, has zero volume. The presence of dissipative elements in a system favors the existence of a stable limit cycle, but does not guarantee it in any way. However, the presence of a limit cycle in a system attests to some form of dissipation.

Since the existence of stable limit cycles for the compass-gait biped has already been demonstrated, the system must be dissipating energy. As the swing stage of the robot is a Hamiltonian system (being equivalent to a frictionless double pendulum) the dissipation must come from the impact equations. The phase space volume contraction and the strong stabilizing effect of the transition equations was pointed out by [20] and was confirmed by [10][9]. In the following, we focus on the characteristics of the impact equations and compute the volume contraction effected by this.

Let \mathbf{q}^{*-} be the state vector of the robot just before the transition. We consider a parallelepiped \mathcal{P}^- based at the vertex \mathbf{q}^{*-} (with edge vectors $\varepsilon_j \mathbf{i}_j$, $j \in \{1, \dots, 4\}$, with ε_j small scalars and \mathbf{i}_j the j^{th} column of identity matrix \mathbf{I}_4). We would like to calculate the change in volume of this parallelepiped (i.e., the “volume” of the ensemble of states just before collision) due to transition. When \mathbf{q}^{*-} is perturbed by an amount $\delta \mathbf{q}^-$, a first order approximation of the state vector just after transition is:

$$\mathbf{q}^{*+} + \delta \mathbf{q}^+ = \mathbf{W}(\alpha^*)(\mathbf{q}^{*-} + \delta \mathbf{q}^-) + \left. \frac{\partial \mathbf{W}(\alpha) \mathbf{q}^{*-}}{\partial \alpha} \right|_{\alpha=\alpha^*} \cdot \delta \alpha \quad (9)$$

Eq. (9) can be written in a compact form as:

$$\delta \mathbf{q}^+ = \mathbf{W}_1(\mathbf{q}^{*-}) \delta \mathbf{q}^- \quad (10)$$

with:

$$\mathbf{W}_1(\mathbf{q}^{*-}) = \begin{pmatrix} \mathbf{J} & \mathbf{0} \\ \left. \frac{\partial \mathbf{H}(\frac{1}{2}(\theta_{n_s}^- - \theta_s^-)) \dot{\boldsymbol{\theta}}^{*-}}{\partial \boldsymbol{\theta}} \right|_{\boldsymbol{\theta}^- = \boldsymbol{\theta}^{*-}} & \mathbf{H}(\alpha^*) \end{pmatrix} \quad (11)$$

In view of Eq. (11), a first-order approximation to the “image” of \mathcal{P}^- through the transition matrix is the polyhedra \mathcal{P}^+ whose edge vectors starting from \mathbf{q}^{*+} are $\varepsilon_j \mathbf{w}_{1,j}$, $j \in \{1, \dots, 4\}$, where $\mathbf{w}_{1,j}$ is the j^{th} column of matrix $\mathbf{W}_1(\mathbf{q}^{*-})$. Since the volume of an n -dimensional parallelepiped is given by the determinant of the matrix whose columns are its n edge vectors[16], the volumes of \mathcal{P}^- and \mathcal{P}^+ are respectively:

$$\text{volume}(\mathcal{P}^-) = \left| \prod_{j=1}^4 \varepsilon_j \right| \quad \text{volume}(\mathcal{P}^+) = \left| \left(\prod_{j=1}^4 \varepsilon_j \right) \cdot \det(\mathbf{W}_1(\mathbf{q}^{*-})) \right| \quad (12)$$

² “hyper” volume element in higher dimensional systems

Therefore a first-order approximation to the change in phase space volume during the transition stage of a steady gait is, using (11) and (12):

$$\frac{\text{Volume}^+}{\text{Volume}^-} = |\det(\mathbf{H}(\alpha^*))| \quad (13)$$

The determinant can be computed as:

$$\begin{aligned} |\det(\mathbf{H}(\alpha^*))| &= |\det((\mathbf{Q}^+(\alpha^*))^{-1}) \det(\mathbf{Q}^-(\alpha^*))| \\ &= \frac{1}{1 + (1 + \beta)^2[\mu + 1 - \cos^2(2\alpha^*)]} \end{aligned} \quad (14)$$

Since μ , β and $1 - \cos^2(2\alpha^*)$ are always positive, $|\det(\mathbf{H}(\alpha^*))| < 1$ which indicates that phase space volumes are always contracted.

It is important to recall that contraction does not imply stability. For example, the volume of a parallelepiped all of whose sides except one are contracted by a factor of two during each transition, while the last side is doubled, will vanish eventually. However the parallelepiped consists of diverging points and will not represent a stable gait.

For a stable limit cycle the rate of contraction describes how fast the neighboring trajectories converge. For the robot model with $\mu = 2$, $\beta = 1$ and $\alpha^* = 15^\circ$ we get $\det(\mathbf{H}(\alpha^*)) = 0.1$. Thus we can say that locally the phase space volumes are contracted by a factor of 10 indicating that the limit cycle is strongly attractive.

Finally let us present two graphical visualizations showing the effect of $\mathbf{H}(\alpha)$ as a mapping between the pre-impact and post-impact joint velocities. In Fig 3 we show this mapping in the 3-dimensional space of joint velocities $\hat{\theta}_s$, $\hat{\theta}_{ns}$, and the interleg angle 2α . The parallelepiped region shown in the figure represents the ensemble of pre-impact robot states with both joint velocities varying from $-100^\circ/\text{sec}$ to $+100^\circ/\text{sec}$ and the interleg angle varying from 0° to 80° . We have taken horizontal (constant interleg angle) slices of this parallelepiped and mapped them through $\mathbf{H}(\alpha)$. The mapped quadrilateral regions are stacked one above another and the stack is superposed on the pre-impact parallelepiped for direct comparison. By comparing the size of a cross-section of the parallelepiped and the size of any of the mapped quadrilaterals in the figure we can clearly see the contraction of the space. Also the figure shows the twist produced in the space by the mapping.

Another way to investigate the behavior of the matrix $\mathbf{H}(\alpha)$ is to observe the evolution of its eigenvalues as the robot parameters continuously change. In Fig. 4(a) we show the moduli of the two eigenvalues of $\mathbf{H}(\alpha)$ as functions of the interleg angle 2α (varying from 0° to 80°) and β (varying from 0.8 to 10). Fig. 4(b) is identical to Fig. 4(a) except that here 2α and μ are the variables, μ varying between 0.3 to 10. In both the figures a typical curve has three separate zones. In the first zone, corresponding to small values 2α , the eigenvalues are real and distinct and their evolution with respect to 2α are given by two separate lines. As the eigenvalues become complex conjugates these two lines merge and begin the second zone. At the end of the second zone the lines separate out reflecting the fact that the eigenvalues have again become real and distinct. This is the third zone. The relative sizes of the zones depend on the parameters μ and β .

Recalling that the determinant of a matrix is equal to the product of its eigenvalues, we can immediately notice the phase fluid contraction caused by $\mathbf{H}(\alpha)$ by reading off the moduli of the two eigenvalues for any given 2α from the plots. One curious thing happens for small values of β ; as the value of α is increased, the modulus of the larger of the two eigenvalues increases rapidly. When $\beta = 0.8$ and $2\alpha = 80$, the larger eigenvalue modulus reaches 1.2, and continues to increase if we go on decreasing β ; for instance, when $\beta = 0.01$ and $2\alpha = 80$, it reaches 97.69. However, the determinant of the matrix is always less than unity thereby guaranteeing volume contraction.

4 Influence of robot parameters on the gait

This section presents the effects of continuous change of the parameters ϕ , μ , and β on the gait of our compass-like biped robot. First we discuss the limitations of a linear model in predicting the robot's long term behavior. Next we point out the general features of the symmetric gaits of the robot – this section mainly consists of a graphical presentation. When one of the parameters exceeds a certain limiting value, we observe bifurcation of the dynamics which we discuss subsequently. Finally we focus on the features of chaotic behavior of the robot gait and calculate the fractal dimension of the strange attractor to which the phase-space trajectory collapses. Since, to our

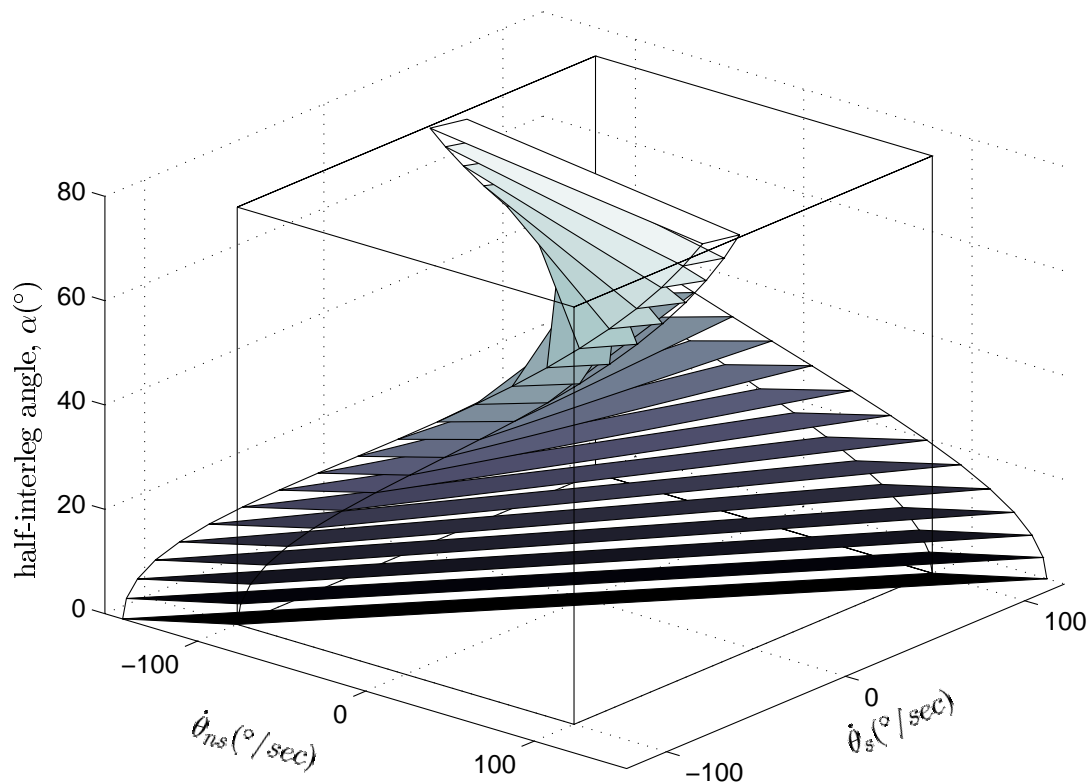


Figure 3: The characteristics of the mapping through the matrix $\mathbf{H}(\alpha)$ demonstrated graphically. The wire frame parallelepiped represents an ensemble of pre-impact robot states (joint velocities $\theta_s^-, \theta_{ns}^+$, and interleg angle 2α). We have taken horizontal (constant interleg angle) slices of this parallelepiped and mapped these square regions through $\mathbf{H}(\alpha)$ to obtain quadrilateral regions of post-impact robot states $\theta_s^+, \theta_{ns}^+$. The quadrilaterals at their respective horizontal positions (their 2α values) are then stacked one above another and the entire stack is superposed on the pre-impact parallelepiped for direct comparison of their sizes. The corresponding vertices of the quadrilaterals for each horizontal position are connected by a line (four lines for four vertices) to show the twist produced by the mapping. A pre-impact square cross-section is mapped to a post-impact quadrilateral of much smaller area illustrating the phase fluid contraction.

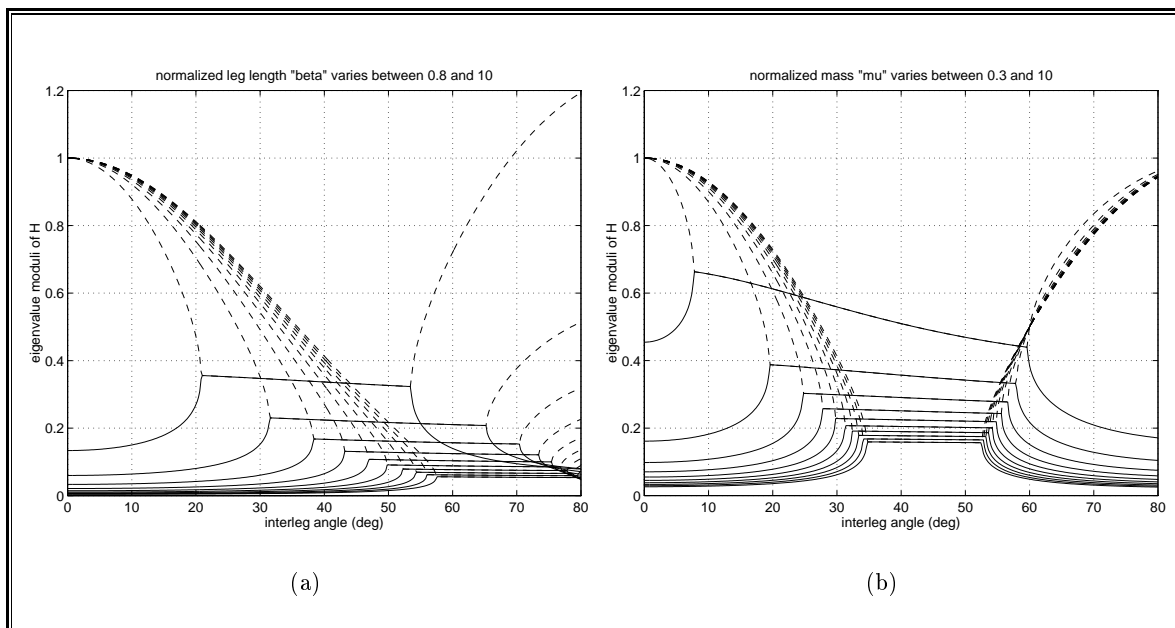


Figure 4: The moduli of the eigenvalues of the transition matrix $\mathbf{H}(\alpha)$ shown as functions of the parameters β (Fig. 4(a)) and μ (Fig. 4(b)). For both the figures, the vertical axis represents the eigenvalue moduli and the horizontal axis is the interleg angle 2α . The volume contraction of phase fluid is proportional to the determinant of $\mathbf{H}(\alpha)$ which is equal to the product of its two eigenvalues. For any 2α , we can visually infer the contraction by reading off the moduli of the two eigenvalues from the plots.

knowledge, there is no analytical method of studying the long-term global behavior of such full-fledged nonlinear and hybrid systems, we adopt numerical techniques for this purpose.

Let us provide certain specifications of the numerical tools that we use. All the simulations presented in this article have been performed using the software Scilab-2.2[33] developed by INRIA³. We have used the routine `ode`, the initial value problem solver with a dedicated stopping time algorithm. In the background `ode` uses the routine `lsodar`, the well-known Livermore solver for ordinary differential equations, with automatic method switching for stiff and non-stiff problems, and with root-finding. The algorithm is guided by two error-threshold parameters called `rtol` and `atol`, the relative and absolute estimated error parameter, respectively. The estimated error in each state is bounded by $\text{rtol} \times \text{abs}(\text{state_variable}(i)) + 0.01 \times \text{atol}$. For our simulations we set `rtol` = 1.d-5 and `atol` = 1.d-7. The particular advantage of this algorithm is that the user is not required to determine if the problem is stiff or non-stiff as the algorithm decides it automatically and switches to the correct mode. The arithmetic precision of the algorithm is 1.d-18.

The stopping time algorithm plays a very important role in our simulation. It is employed to precisely detect the contact of the swing leg with the ground. The algorithm is a nonlinear root finder which finds only those roots for which some function, which in our case is the distance between the robot leg and the ground, changes sign in the interval of integration. When a root is found it is located only to within an error of $\text{hmin} = 100 \times \text{uround} \times \max(\text{abs}(x_0), \text{abs}(x_1))$, where `uround` is the unit roundoff of the machine and x_0, x_1 are the endpoints of the interval where roots are sought. The contact between the robot and the ground is detected with a typical precision of 1.d-17m.

4.1 Limitations of the linear model

One of the most important pieces of information necessary for such numerical techniques is the size of the basin of attraction of the stable limit cycle. If the initial states of the robot are within

³ftp site: <ftp://ftp.inria.fr/INRIA/Scilab/>
 Web page: <http://www-rocq.inria.fr/scilab/>
 e-mail: scilab@inria.fr

the basin of attraction, they will eventually converge to the limit cycle. In order to guess such initial conditions we have tried using the initial states calculated from the analytical solution of the linearized robot model [12]. Similar to the method proposed in [26], we linearized the swing stage equations around the equilibrium $\mathbf{q} = \mathbf{0}$ which represents a motionless vertical configuration of the robot. The transition equations were added and a periodicity condition of the gait was employed to analytically obtain initial states that lie precisely on a periodic solution of the linear model.

If nonlinearities in the equations are not too influential these initial states will perhaps belong to the attraction basin of the limit cycle of the actual nonlinear model and the solution will eventually converge to it after the transients die down. Our simulations showed that this approach is successful for small ϕ and small β . Specifically, for any $\mu \in [0.1, 10]$, this method leads us to a limit cycle

$$\begin{aligned} &\text{for } \beta < 4.8 \text{ when } \phi = 0.25^\circ, && \text{for } \beta < 1.5 \text{ when } \phi = 3^\circ, \\ &\text{for } \beta < 2.9 \text{ when } \phi = 1.5^\circ, && \text{for } \beta < 1 \text{ when } \phi = 4^\circ. \end{aligned}$$

Interestingly enough μ does not affect the success or failure of this method.

In situations where prediction based on the linear model failed, we choose as the initial states, a state vector \mathbf{q} on the known nonlinear limit cycle of a robot whose parameters (ϕ, μ, β) are close to those of the robot under study. Given the relatively small dimension of the state space this method worked satisfactorily.

4.2 Symmetric gaits

This section is an album of plots (Figs. 5, 6, 7) presenting the evolution of pertinent *gait descriptors* as functions of the three parameters during the symmetric gait regime of the robot. As opposed to a parameter which can be directly altered, a gait descriptor is an observed (measurable or computable) quantity which cannot be modified directly but is indirectly influenced by the parameters. The gait descriptors that appear the most meaningful to us for this study are the state variables \mathbf{q} , the half inter-leg angle at touchdown α , the step period T , the average speed of progression v , the total mechanical energy of the robot E and the loss of mechanical energy ΔE due to impact.

The evolution of the gait descriptors is presented in the form of so-called *bifurcation diagrams* [1][14][17]⁴. Figs. 5(a) to 5(f), 6(a) to 6(f) and 7(a) to 7(f) present the evolution of the gait descriptors T , α , $\dot{\theta}_s$ (at the beginning of a step), v , E and $\frac{\Delta E}{E}$ as functions, respectively, of the parameters ϕ , μ and β . The results show that both the step period and the step length of the robot increase with an increase in any of the three parameters. The robot's translational velocity, however, increases with ϕ and μ but decreases with β . The overall behavior of the robot can be summarized qualitatively as follows:

	T	L	E	v
when $\phi \nearrow$	\nearrow	\nearrow	\nearrow	\nearrow
when $\mu \nearrow$	\nearrow	\nearrow	\nearrow	\nearrow
when $\beta \nearrow$	\nearrow	\nearrow	\searrow	\searrow

Some interpretations are in order here. Let us consider the evolution of total mechanical energy E of the robot in response to parameter changes. As the ground slope ϕ increases the potential energy PE of the robot available per step slightly increases. The kinetic energy KE , being roughly proportional to $\|\dot{\theta}\|^2$, increases also, see Fig. 5(c). As a consequence the total energy E increases, Fig. 5(e). An increase in β , however, causes a net decrease in E , see Fig. 7(e) and can be explained as follows. An increase in β results in a lowering of the center of mass of the robot, which lowers PE available per step and increases the step period. The latter results in a decrease in the average velocity of the robot (Fig. 7(d)). The increase in KE caused by the small increase in the $\dot{\theta}_s$ cannot compensate for the decrease in PE and consequently lowers E . Conversely, an increase in μ , which results in raising the center of mass of the robot, increases E .

It is interesting to look at the effect of a parameter change on the evolution of entire limit cycles as shown in Figs. 5(g), 6(g) and 7(g). In response to an increase in ϕ the limit cycle expands along both the axes, see Fig. 5(g), implying an increase in the range of joint angle and joint velocity. The limit cycles are compressed along the joint velocity axis for an increase in the parameters μ and β (Figs. 6(g) and 7(g)). A shorter reach of the limit cycle along the joint velocity axis means a

⁴Discussion of bifurcation and asymmetric gaits, represented by the regions beyond the branched sections in the bifurcation diagrams of Figs. 5, 6, 7, is postponed until the next section.

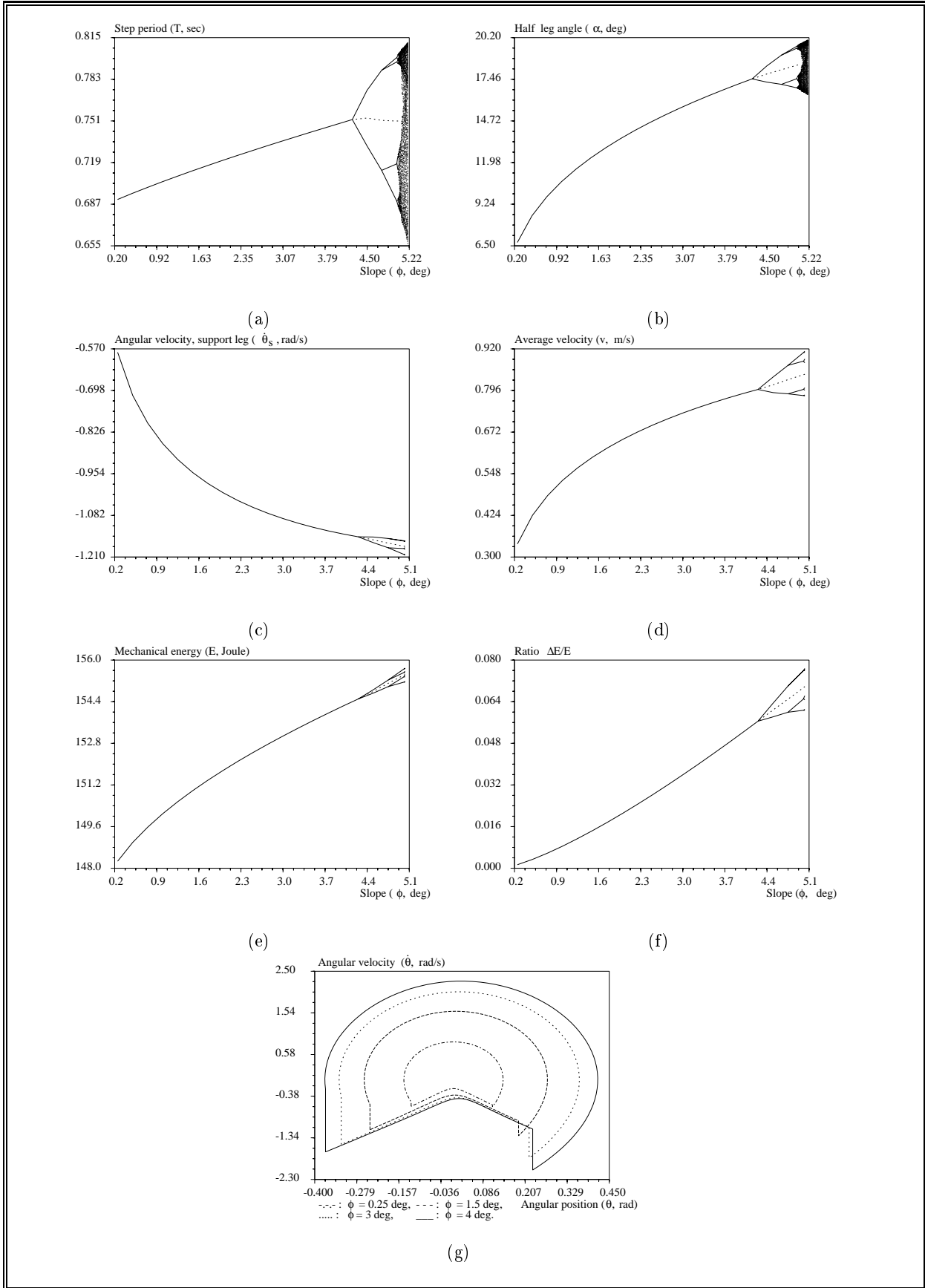


Figure 5: Bifurcation diagrams showing the variation of the gait descriptors with respect to ground slope ϕ : a) step period T , b) half inter-leg angle α , c) angular velocity of the support leg $\dot{\theta}_s$, d) average speed of progression v , e) mechanical energy E , f) ratio $\frac{\Delta E}{E}$, g) Phase plane limit cycles for $\phi = 0.25^\circ, 1.5^\circ, 3^\circ$ and 4° .

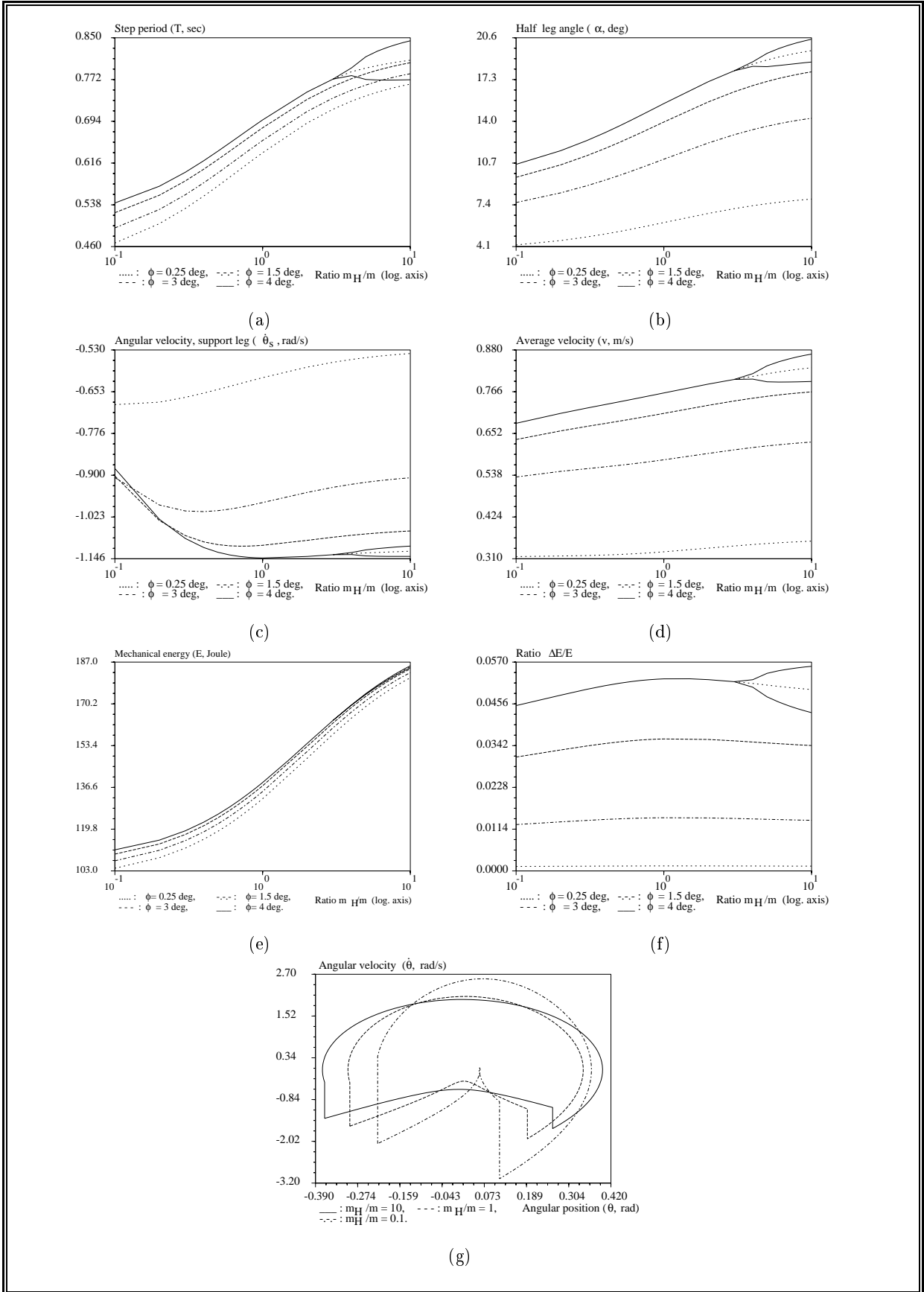


Figure 6: Bifurcation diagrams showing the variation of the gait descriptors with respect to mass ratio μ : a) step period T , b) half inter-leg angle α , c) angular velocity of the support leg $\dot{\theta}_s$, d) average speed of progression v , e) mechanical energy E , f) ratio $\frac{\Delta E}{E}$, g) Phase plane limit cycles for $\mu = 10, 1$ and 0.1 ($\beta = 1, \phi = 3^\circ$). For Figs. 6(a) to 6(f) $\beta = 1, \phi = 0.25^\circ, 1.5^\circ, 3^\circ$ and 4° .

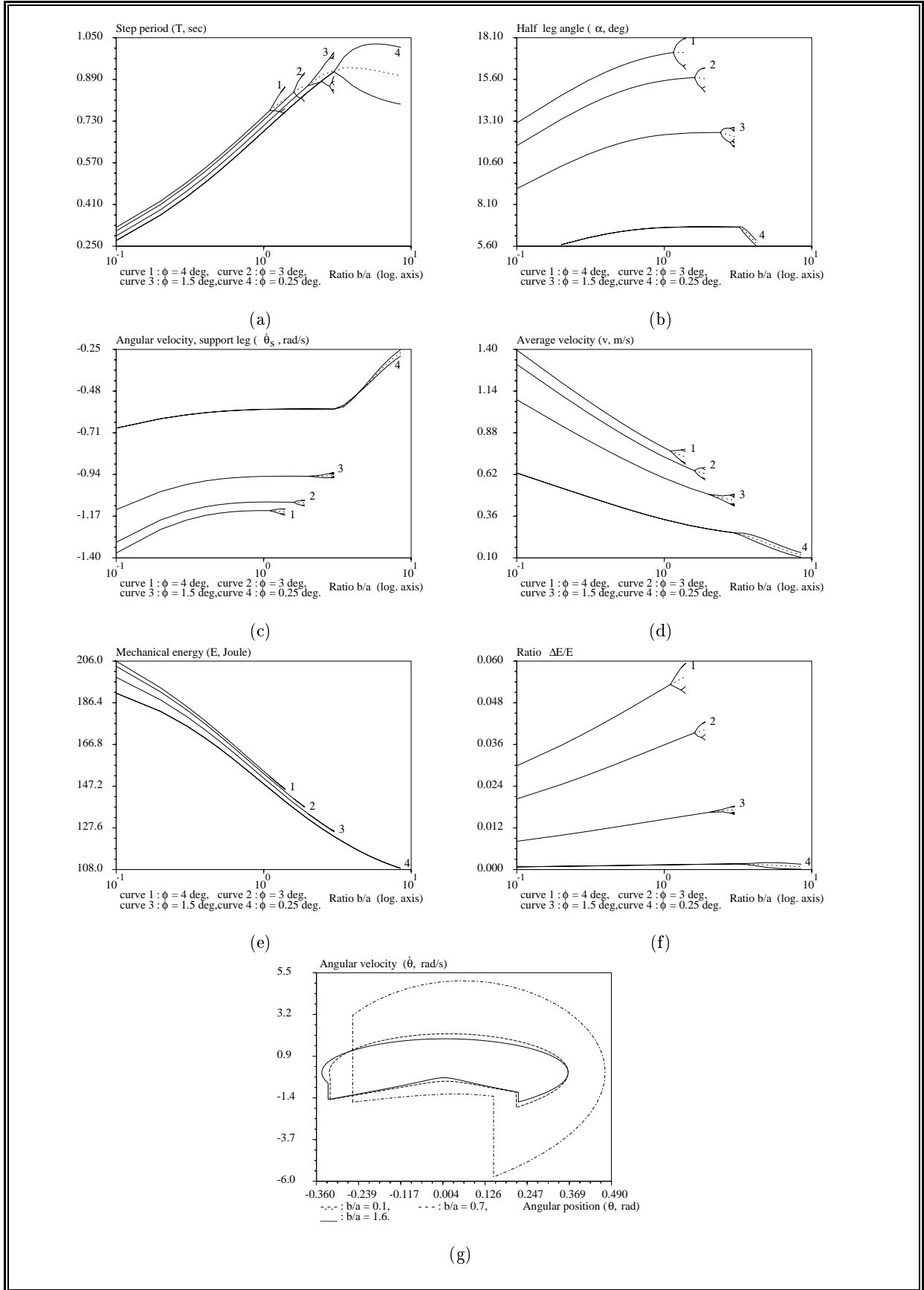


Figure 7: Bifurcation diagrams showing the variation of the gait descriptors with respect to length ratio β : a) step period T , b) half inter-leg angle α , c) angular velocity of the support leg $\dot{\theta}_s$, d) average speed of progression v , e) mechanical energy E , f) ratio $\frac{\Delta E}{E}$, g) Phase plane limit cycles for $\beta = 0.1, 0.7$ and 1.6 ($\mu = 2, \phi = 3^\circ$). For Figs. 7(a) to 7(f) $\beta = 1, \phi = 0.25^\circ, 1.5^\circ, 3^\circ$ and 4° .

smaller maximum joint velocity but does not necessarily mean a slower robot. We see in Fig.6(d) that an increase in μ is associated with an increase in the average speed of progression v .

It is interesting to note that for a given triplet (ϕ, μ, β) , we have never identified more than one stable steady gait. Moreover, except in Fig. 6(c) and Fig. 6(f) all the gait descriptors evolve monotonically in the symmetric gait regime. This reinforces our suspicion that, for a given robot with specified parameters μ and β the ground slope ϕ *uniquely* defines all gait variables. Although we cannot claim this as a proof, the property of monotonic evolution of the variables is nevertheless exploited in [6], [10] and [11] in formulating control strategies for the compass. It was observed that a scalar control law which seeks to converge the mechanical energy of the “actively controlled” compass to that corresponding to a known passive gait ensures, in fact, the convergence of *all* the state variables of the robot.

For our nominal robot model we have found symmetric gaits until $\phi = 4.37^\circ$ at which point the gait bifurcates to a 2-periodic gait. The model studied in [9] exhibits symmetric gaits until $\phi = 0.865^\circ$.

4.3 Period-doubling bifurcation

We noticed in Figs. 5 and 6 that for the range of variations of the parameters considered in this study an increase in ϕ and β cause a bifurcation in all the gait descriptors. Bifurcation was also observed for higher values of μ especially when coupled with higher values of ϕ (Fig. 7).

The occurrence of period-doubling bifurcation can be studied by means of the Poincaré first return map [1][17] constructed in the neighborhood of a stable limit cycle. The eigenvalues of the Jacobian matrix of this map are indicators of the bifurcation. For a stable symmetric gait, the eigenvalues are within the unit circle. Modification of a parameter alters the eigenvalues, and at the bifurcation point at least one crosses the unit circle. Recalling that the unit circle crossing of the eigenvalues is also an indication of instability in the symmetric gait, we may say that at the bifurcation point the symmetric gait becomes unstable. In fact, the eigenvalues of the first return map of the stable post-bifurcation gait, which correspond to those of the “second” return map of the pre-bifurcation symmetric gait, will remain inside the unit circle.

The particular fashion in which an eigenvalue crosses the unit circle determines the type of structural instability that the system undergoes. Flip bifurcation[36], which is the case here, corresponds to an eigenvalue leaving the unit circle along the real axis, with a negative real part. Fig. 8 presents the evolution of the eigenvalues of the Jacobian of the biped’s Poincaré map as a function of ϕ . All are real, and one of them actually reaches the value -1 when the first bifurcation point is reached at $\phi = 4.37^\circ$.

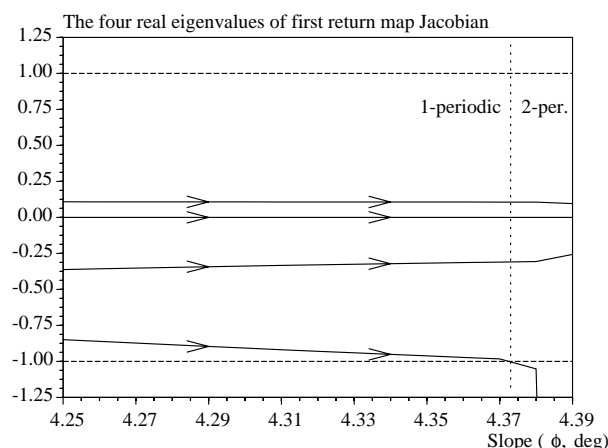


Figure 8: *Transition from a 1-periodic to a 2-periodic steady gait: behavior of the eigenvalues of the Jacobian matrix of the robot’s Poincaré map.*

As a consequence of the period-doubling bifurcation the limit cycle becomes 2-periodic and the robot gait becomes asymmetric with a shorter step and a longer step. The occurrence of bifurcation is shown in Figs. 5, 6, 7 by the emergence of two branches in the curves, each associated with one

of the two dissimilar steps and describing its characteristic variables. Since bifurcation involves the state of the system and since all the gait descriptors, in turn, depend on the robot states, the occurrence of bifurcation is simultaneously manifested in all the gait descriptors⁵.

On further increasing the parameters, the robot gait may experience a further period-doubling, giving rise to a 4-periodic limit cycle. This phenomenon, repeated ad infinitum, is called a *period doubling cascade* and is recognized as one of the possible routes leading to chaos. Regardless of the parameter considered, we observe that the successive period doublings occur after progressively smaller intervals of parameter variation. This is expected in view of general results on period doubling cascades[1].

Period doubling cascades leading to chaotic behavior have already been observed for passive planar hopping robots which possess a smaller dimension than that of the compass. 2^n -periodic gaits, termed as “limping gaits,” were observed and analyzed for hopping robots [31][37], [25][29][8][22].

In Fig. 9 we introduce a novel way of capturing the behavior of the biped during a period doubling cascade ensuing from the parameter ϕ (other parameters are kept constant at $\mu = 2, \beta = 1$). The figure plots the first return map of θ_{ns} . For a 1-periodic robot gait θ_{ns} is the same in every

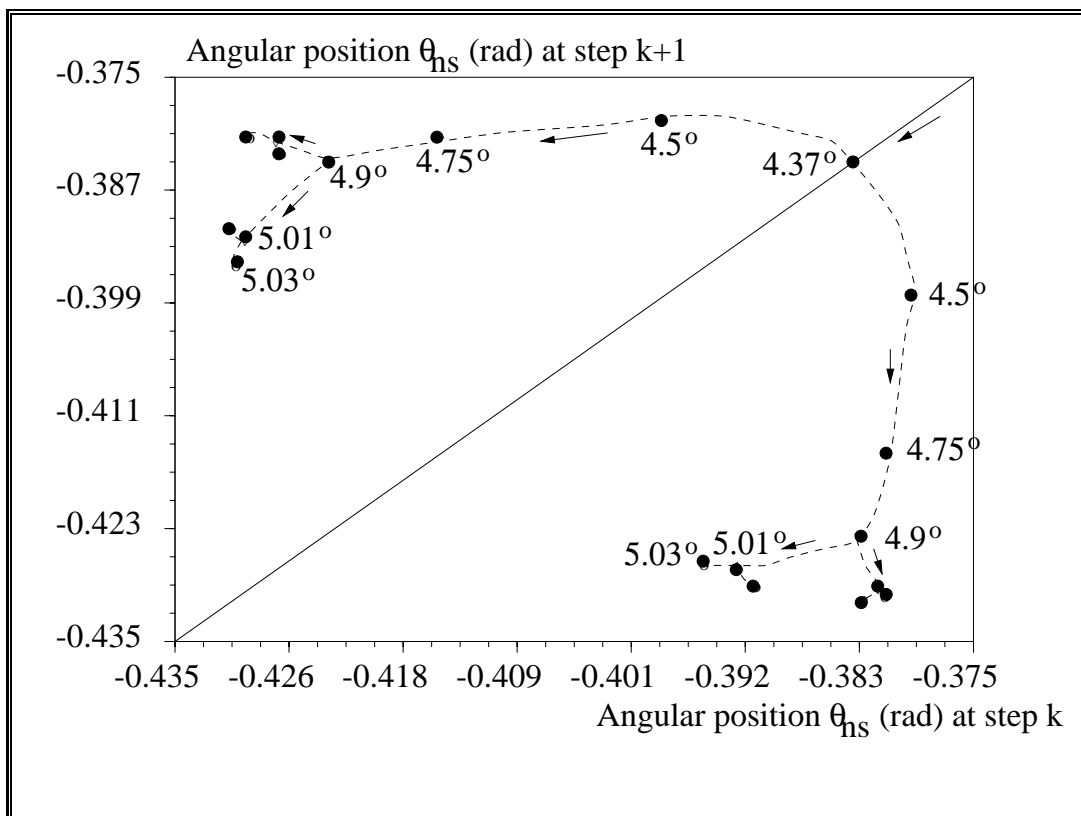


Figure 9: *First-return map of 2^n -periodic steady gaits $n \in \{0, 1, 2, 3\}$.* In response to a variation of the ground slope from $\phi = 4.37^\circ$ to 5.03° the robot gait undergoes three successive bifurcations. Here we show the Poincaré map of the non-support leg angle θ_{ns} . Until the first bifurcation occurs at 4.37° the map is a point on the 45° line.

step. This gait is therefore represented by a point on the 45° line. As we change the ground slope, this point moves along the 45° line from the right-hand top corner of Fig. 9, as indicated by the arrow.

The first period doubling occurs at $\phi = 4.37^\circ$ when the gait turns 2-periodic and is therefore represented by 2 points. Just after the first bifurcation the 2 representative points differ only slightly from that of the 1-periodic gait from which they originate. The two steps are therefore very similar to the steps of the symmetric gait. On further changes in the parameter the two

⁵The occurrence of bifurcation may not, however, be equally prominent in all the bifurcation diagrams because of the effect of scaling. Thus, whereas we can clearly see a bifurcation of the step period in Fig. 5(a), the corresponding bifurcation of the mechanical energy is much less prominent in Fig. 5(e).

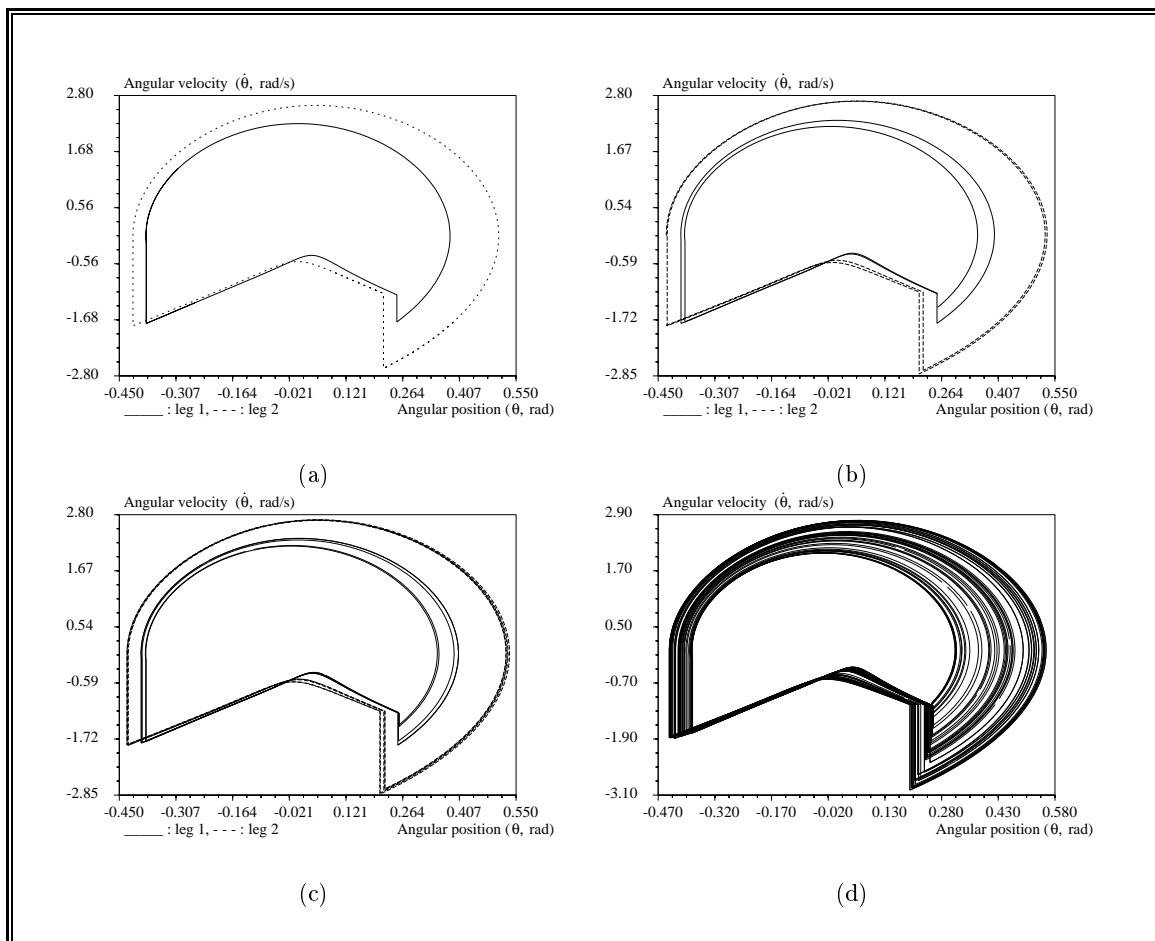


Figure 10: *Phase plane limit cycles of a) 2-periodic steady gait ($\phi = 4.75^\circ$), b) 4-periodic steady gait ($\phi = 5^\circ$), c) 8-periodic steady gait ($\phi = 5.02^\circ$) d) chaotic gait associated with one leg, 100 robot steps, ($\phi = 5.2^\circ$). For all the 4 subplots $\mu = 2$, $\beta = 1$.*

representative points move away from the 45° line along the two branches shown by dotted lines in Fig. 9. It follows that one step length is slightly longer and the other slightly shorter than those of the corresponding symmetric gait. As we increase the slope the longer step is further elongated and the shorter step further shortened.

This continues until a second period doubling occurs at $\phi = 4.9^\circ$ when each branch gives rise to two sub-branches. In this 4-periodic gait the 4 different steps are visited in the same order with a long step always followed by a short step. The last clearly identifiable bifurcation occurs when $\phi = 5.01^\circ$ as the robot gait becomes 8-periodic.

The period doubling cascade may also be observed using phase plane diagrams. The phase plane diagram for a symmetric gait was already shown in Fig. 2 which is a single-loop closed trajectory repeated after two robot steps. During one step the considered leg is in the swing stage and during the following one, it is in the support stage. Since the gait is symmetric, the robot legs are indistinguishable and the phase plane cycles of the two legs are identical.

In case of a 2-periodic gait, since all state variables are identical after every two steps, the phase plane limit cycle associated with one leg is still a single-loop closed trajectory repeated after two robot steps, see Fig. 10(a). However, since the gait is asymmetric, the limit cycles associated with the legs are no longer identical.

In case of 2^n -periodic gaits, all the state variables repeat themselves after every 2^n steps. The phase plane diagram associated with one leg is therefore a 2^{n-1} -loop closed trajectory repeated after every 2^n steps, distinguishable from the phase plane diagram of the other leg. The visual inspection of the phase plane diagrams of the 4-periodic and the 8-periodic gaits (Figs. 10(b) and 10(c), respectively) correctly indicates that they resulted from the bifurcation of respectively the

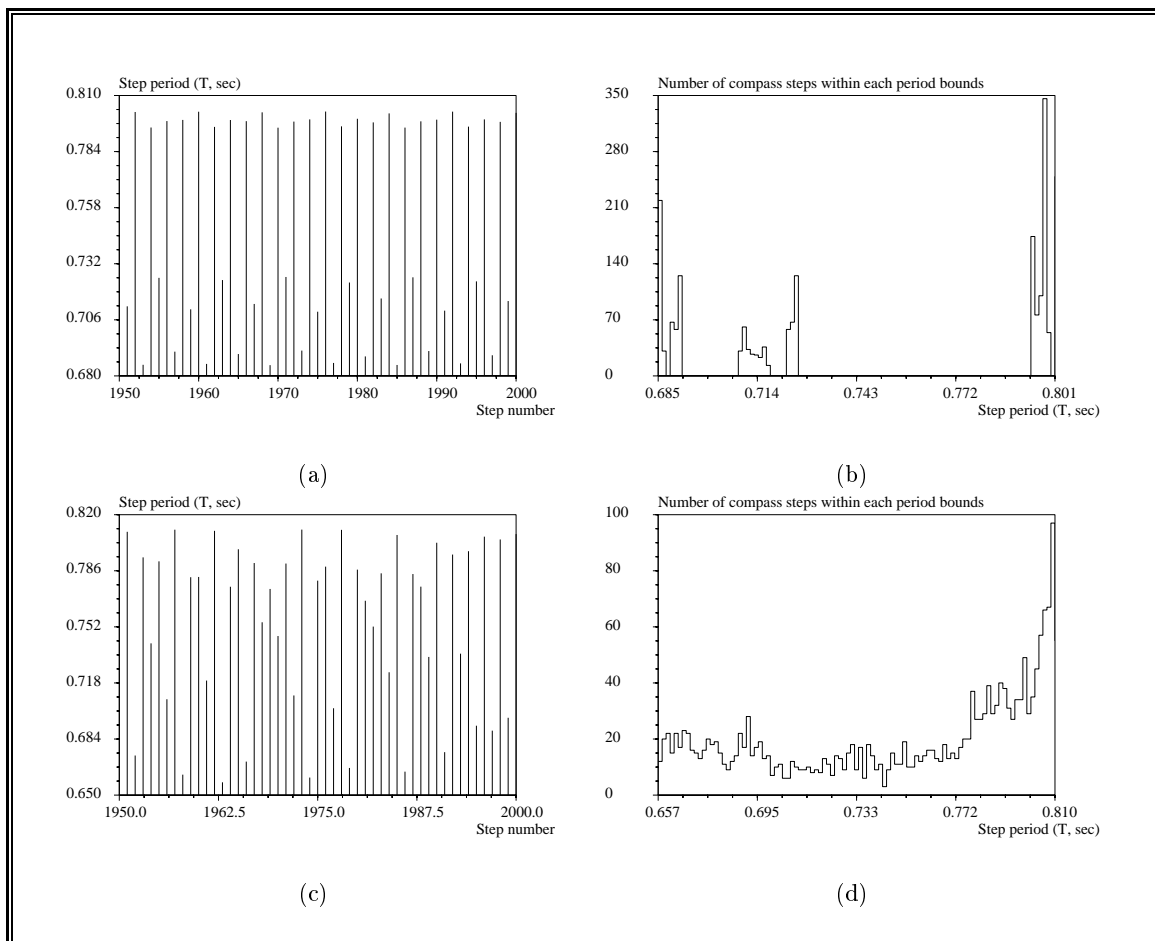


Figure 11: 2^n -periodic steady gait, n large: a) periods of 50 consecutive steps and b) histogram of the periods of 2000 consecutive steps for $\phi = 5.04^\circ$. Chaotic gait: c) periods of 50 consecutive steps and histogram of the periods of 2000 consecutive steps for $\phi = 5.2^\circ$. For all the 4 subplots $\mu = 2$ and $\beta = 1$.

preceding 2-periodic and the 4-periodic gaits.

4.4 Chaotic gaits

The chaotic gait is an extreme case of the asymmetric gait and is characterized by a complete disappearance of order in a system. During a chaotic gait on a given slope, the states, and consequently the gait descriptors, of the biped robot never completely repeat themselves. Chaotic gaits are represented in the bifurcation diagrams by a continuous distribution of points. We explicitly show this on Figs. 5(a) and 5(b) and omit them in the other bifurcation diagrams for the sake of clarity.

For our compass-gait robot the 8-periodic gait is exhibited until $\phi = 5.03^\circ$. If ϕ is further increased, several period doublings take place very quickly and starting from $\phi = 5.04^\circ$ we are unable to detect any periodicity in the motion of the robot. What we mean becomes clearer from Fig. 11(a) which shows 50 consecutive step periods. Although none of these periods are exactly equal, a histogram, i.e., the frequency of occurrence of a small range of step periods vs. the range, reveals 4 major clusters, Fig. 11(b). This indicates the remnants of some order in the system.

Beyond $\phi = 5.04^\circ$ all indicators of order continue to disappear. Fig. 11(c) shows the step periods for 50 consecutive steps and 11(d) shows a frequency histogram of 2000 steps for $\phi = 5.2^\circ$, which is the steepest slope for which the nominal model showed a steady gait. No order in any of the gait descriptors can be detected at this slope. The latter figure shows the presence of “broad-band frequency,” a key feature of chaos. Figs. 10(d) shows the associated phase plane diagram. The robot does not exhibit limit cycle behavior anymore but the trajectories stay on a *strange attractor*

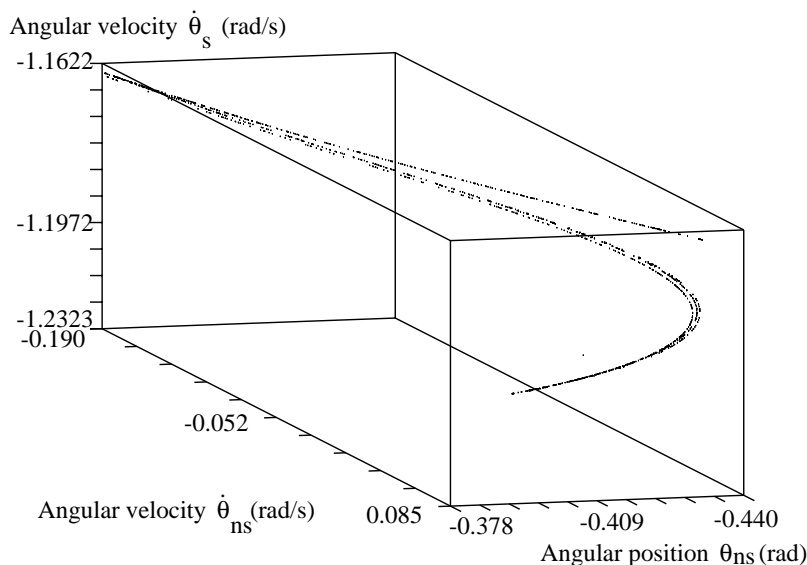


Figure 12: *3D Poincaré section of chaotic gait*: section taken along $\theta_{ns} + \theta_s = -2\phi$, i.e., at the beginning of a swing stage ($\phi = 5.2^\circ$, $\mu = 2$, $\beta = 1$).

which is a manifold of a lower dimension in the phase space.

Following [9] we show a Poincaré section of the strange attractor in Fig. 12. The hyper-plane in the phase-space on which the points of repeated crossings of the phase trajectory forms the Poincaré map is described by $\theta_s = -2\phi - \theta_{ns}$. Physically this hyper-plane corresponds to the beginning of the swing stage. Strange attractors of dynamic systems are generally known to possess a *fractal* or non-integer dimension. We can observe that the Poincaré section consists of multiple closed packed lines separated by empty spaces. The entity is therefore neither a line nor a surface and should have a dimension between 1 and 2.

A numerical procedure[1] was employed to compute the fractal (Hausdorff-Besicovitch) dimension of the strange attractor⁶ whose Poincaré section is depicted in Fig. 12. For the robot with a 4-dimensional state-space, the fractal dimension of the strange attractor was found to be 2.07. The attractor is thus dimensionally close to a Euclidean plane. This is a consequence of the strong phase space volume contraction observed in Section 3.4.

The gradual progression of the robot gait to the chaotic regime is well depicted in the first return maps of $\theta_{ns,k+1} = f(\theta_{ns,k})$ shown in Figs. 13(a) to 13(d). When $\phi = 5.03^\circ$, the gait is 8-periodic and its first return map consists of 8 points as was shown in Fig. 9. At $\phi = 5.04^\circ$, the first return map still consists of 8 distinguishable clusters of points (Fig. 13(a)). Through multiple period doubling bifurcations this 8-periodic gait gives rise to a 2^n -periodic gait with a large n . This gait still preserves some similarity with the 8-periodic gait from which it originates. For example, step order is still preserved and θ_{ns} always visits the 8 clusters, shown in Fig. 13(a), in the same order. In this order a large θ_{ns} (i.e., $|\theta_{ns}| > .4$ rad) is always followed by a small θ_{ns} (i.e., $|\theta_{ns}| < .4$ rad).

When $\phi = 5.08^\circ$, the 8 clusters of points merge into 2 larger packs, see Fig. 13(b). Some order is still preserved, since a large θ_{ns} is still always followed by a small one. The same property still holds for $\phi = 5.12^\circ$, but in this case the first return map appears as a continuum of points (Fig. 13(c)). We are therefore very close to the “broad-band frequency” characteristic typical of chaotic behavior. Finally, when $\phi = 5.2$, we observe that predictability and periodicity have been completely destroyed, since a large θ_{ns} can be followed by another large one. The layered structure of the strange attractor can also be guessed from the first return map.

It is extremely interesting to note that the first return maps of all of the robot gait descriptors look remarkably similar. For instance, the first return map of the step period T (Fig. 14) looks like a scaled and rotated first return map of θ_{ns} (Fig. 13(d)). With this we can suggest that all the

⁶The fractal dimension calculated by this numerical algorithm provides a lower bound for the Hausdorff-Besicovitch dimension. It is an approximate, but close, estimation of it.

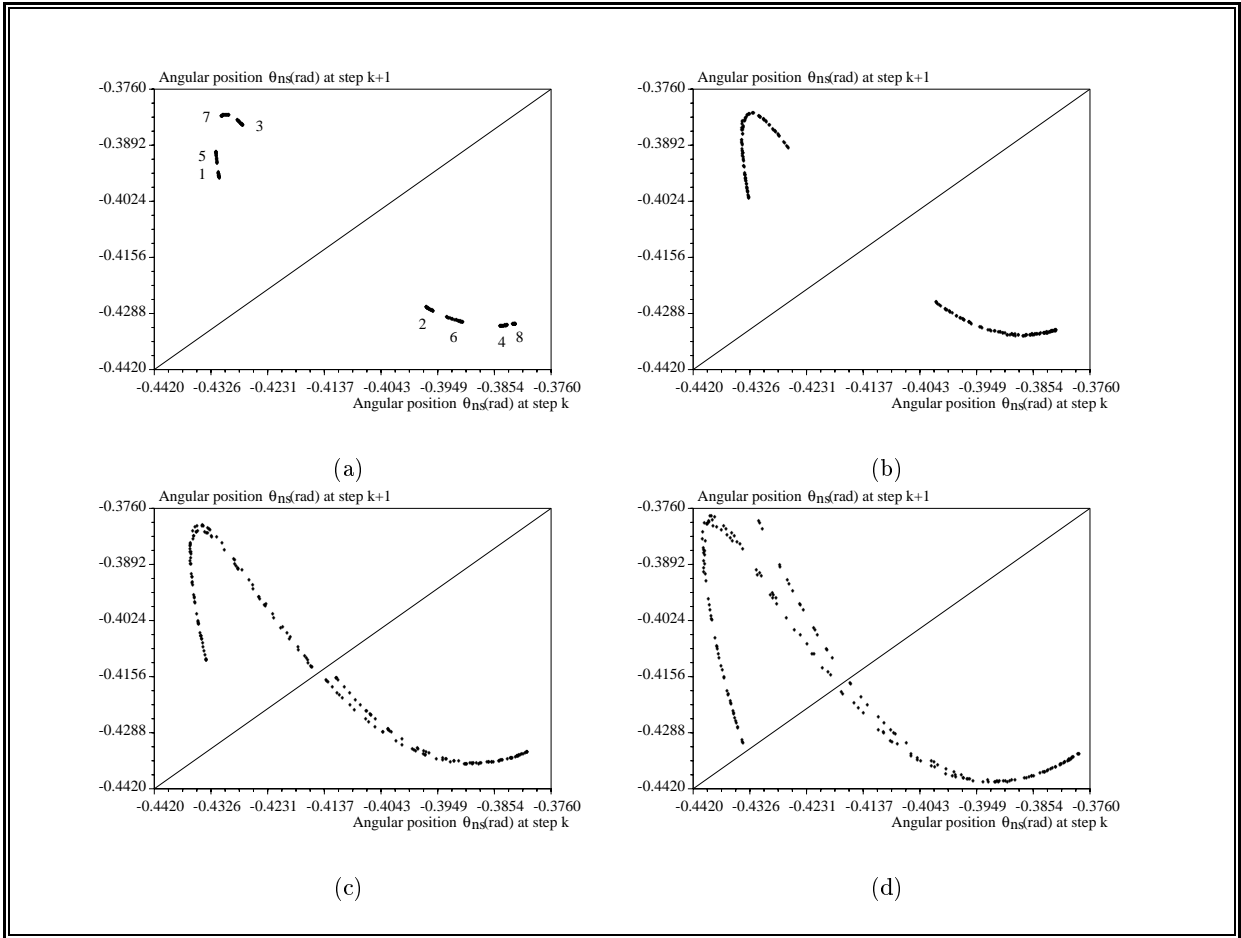


Figure 13: *First return map of $\theta_{n,s}$* : a) 2^n -periodic gait, n large ($\phi = 5.04^\circ$), b) 2^n -periodic gait, n very large ($\phi = 5.08^\circ$), c) approaching chaotic gait ($\phi = 5.12^\circ$), d) chaotic gait ($\phi = 5.2^\circ$). For all the 4 subplots $\mu = 2$, $\beta = 1$.

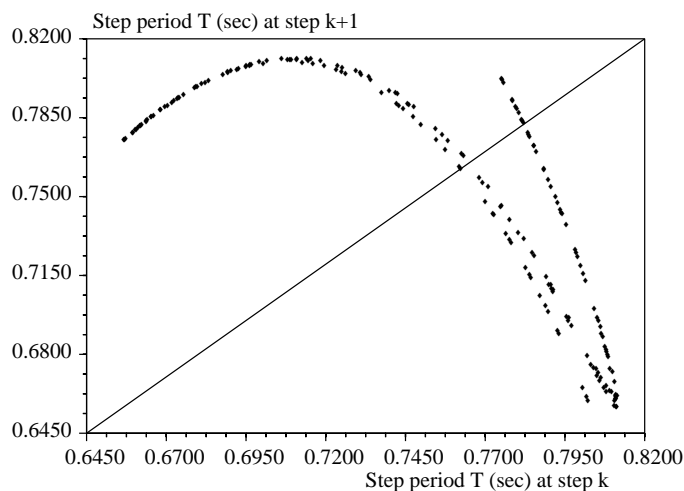


Figure 14: *First return map of T : steady chaotic gait ($\phi = 5.2^\circ$, $\mu = 2$, $\beta = 1$).*

characteristics of the passive chaotic gait of our robot are somehow ensclosed in the shape of its first return map, which can be viewed as a signature of the chaotic gait.

An important characteristic of chaotic motion is the exponential divergence of nearby trajectories [17]. The phase space trajectories of our biped robot exhibit this behavior and this section ends with a presentation of this fact. Figs. 15(a) and 15(b) show the divergence of trajectories initiating from nearby phase space points and continuing for 2 and 12 steps, respectively. The initial states of the two trajectories are $\mathbf{q} = [-0.3829 \ 0.2039 \ -0.1635 \ -1.1622]^T$, corresponding to the dashed line, and $\mathbf{q} = [-0.3819 \ 0.2039 \ -0.1635 \ -1.1622]^T$, corresponding to the solid line. Even after two steps the difference in the trajectories is clearly identifiable and after 12 steps the trajectories bear no semblance to each other although they lie on the same attractor.

5 Dampers improve gait stability

Taking a cue from the connection between gait stability and energy dissipation we studied the effect of placing passive damping elements in the robot's hip joint. A significant improvement of the gait stability and overall gait versatility was achieved by this without violating the "passive" status of the robot. The damper effects a continuous dissipation of energy in the robot in addition to the energy dissipated intermittently during ground impact. Although even a linear damper may increase the range of slopes on which steady gaits exist, we obtained more encouraging results with quadratic dampers. It is possible to consider the damper coefficient as another parameter affecting the robot gait. However we give it a special status here because of its obvious connection to control laws. Indeed, the passive quadratic damper placed in the robot hip joint can be easily replaced by a motor implementing the same physical law. The damper generates a hip joint torque $u_H \propto -\dot{\theta}_H^2 \text{sign}(\dot{\theta}_H) = -(\dot{\theta}_{ns} - \dot{\theta}_s)^2 \text{sign}(\dot{\theta}_{ns} - \dot{\theta}_s)$.

The presence of a damper profoundly alters the passive gait of the robot on a given slope⁷. In Fig. 16 we show three different limit cycles of the robot on a 4° slope – one for the damper-less gait (solid line) and the other two corresponding to two different quadratic dampers (the dashed line for $0.08 \text{ N-m}/(\text{rad/sec})^2$ and the innermost dotted line cycle for $0.15 \text{ N-m}/(\text{rad/sec})^2$).

A robot equipped with a damper may exhibit steady gaits for a larger range of slopes. Fig 17 shows the steady stable gait (asymmetric) for a 10° slope obtained with a quadratic hip damper with a coefficient $0.23 \text{ N-m}/(\text{rad/sec})^2$. For a damper-less robot no gait cycle was found beyond 5.2° slope.

Fig. 5 shows the KE vs PE plots of the robot during a few cycles on 4° slope – Fig. 18(a)

⁷Dampers may increase the size of the limit cycle's basin of attraction for a given slope, but a better tool for estimating the size of the basin is needed to prove it.

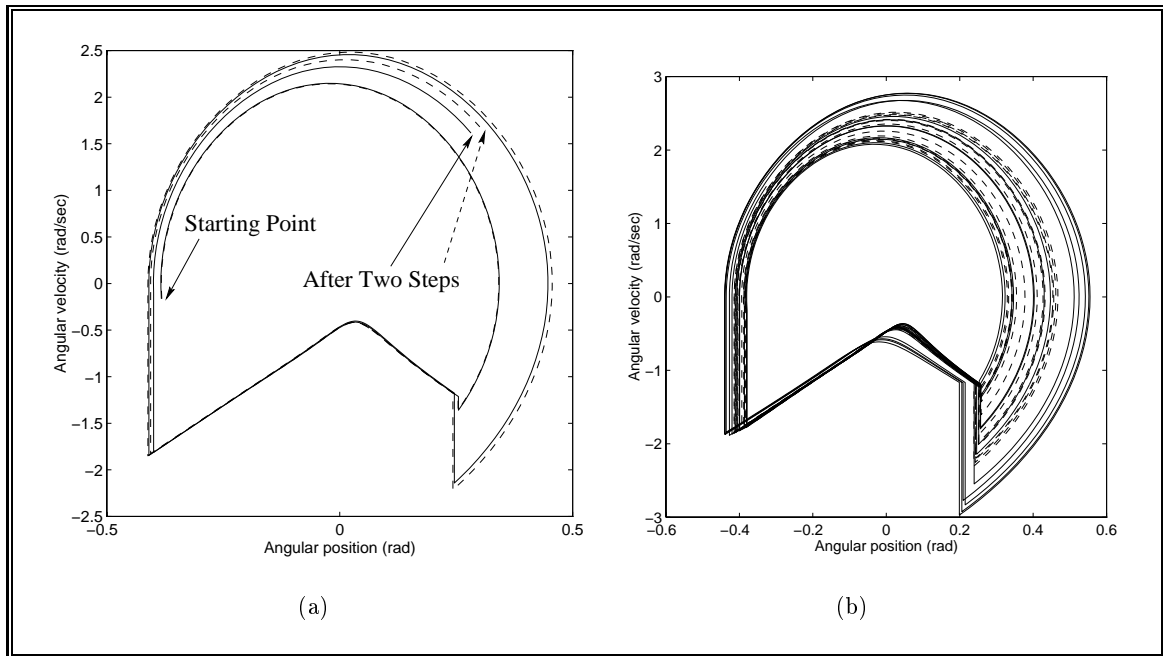


Figure 15: The divergence of nearby trajectories in the phase plane of a biped robot, a phenomenon normally observed in a system with chaotic dynamics. The initial $\dot{\theta}_{n,s}$ between the two trajectories differ by 0.001 rad, the other three state variables being exactly identical. Even after only two steps the difference between the trajectories (shown in solid and dotted lines) is clearly identifiable (a). After 12 steps (b) the trajectories bear no resemblance to each other although they lie on the same attractor.

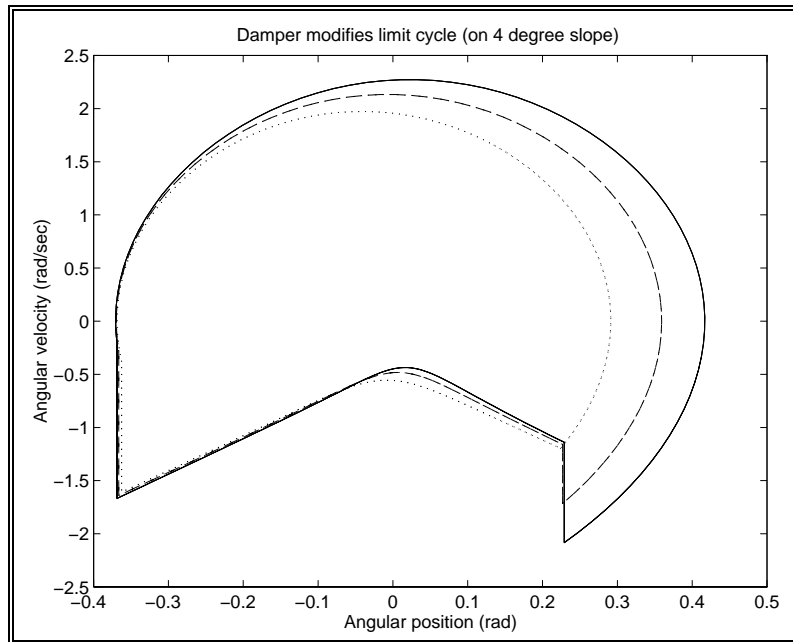


Figure 16: Three different limit cycles for gaits on a 4° slope. The largest (solid line) corresponds to damper-less motion. The other two cycles are obtained by placing quadratic dampers of coefficients $0.08 \text{ N-m}/(\text{rad/sec})^2$ (the dashed line) and $0.15 \text{ N-m}/(\text{rad/sec})^2$ (the innermost dotted line) in the hip joint of the robot.

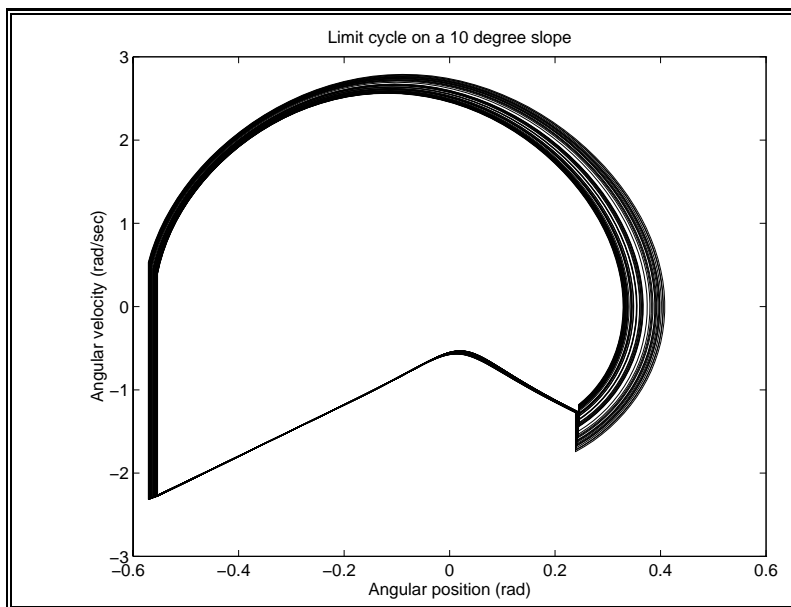


Figure 17: The figure shows the phase diagram of the compass robot with a passive quadratic hip damper (with a coefficient $0.23 \text{ N-m}/(\text{rad/sec})^2$) walking down a 10° slope with a steady gait.

corresponds to the damper-less motion and Fig. 18(b) corresponds to the motion with a $0.15 \text{ N-m}/\text{rad/sec}$ damper. Let us first concentrate on the first figure. As reported in [10] the KE vs PE plot of a damper-less compass robot consists of two straight lines – a constant PE horizontal line representing the ground impact and an inclined line representing the swing stage. The conservation of total mechanical energy of the robot during the swing stage ensures that the inclined line makes a 135° angle with the KE axis. In Fig. 18(a) we see that the PE of the robot decreases by a constant amount at every step. For a steady gait precisely this amount of KE is absorbed during the ground impact.

In the presence of a damper the situation is different. Since the damper continuously dissipates energy during the swing stage, the latter is no longer Hamiltonian and is therefore not represented by a single inclined line. It becomes a curve, the exact nature of which depends on the robot dynamics and the damper coefficient, see Fig. 18(b). In order to exhibit a steady gait the PE lost by the robot during a step must be exactly equal to the *sum* of the energy absorbed during the ground impact and the energy absorbed by the damper during the swing stage. The ground impact phase remains unchanged and is represented by a horizontal line.

In Fig. 19 we visualize the differences in the energy dynamics for the gaits of a robot with and without damper. The figure plots KE vs PE vs (KE+PE) during one gait cycle. The value of PE in this case is re-initialized at each touchdown such that for a steady gait it is a cyclic quantity and is not monotonously decreasing. For a robot without any damper the total energy (KE+PE) is constant during the swing stage and is thus represented by a horizontal line shown at the bottom of this figure. In a cyclic gait the robot repeatedly traces this line. With a damper dissipating energy, the quantity (KE+PE) continuously changes during the motion of the robot and is shown by the superposed closed curve. The straight line joining the extreme right hand corner of the curve to its upper portion represents the instantaneous kinetic energy absorption due to the ground impact coupled with a simultaneous shift of the coordinate frame to re-initialize PE. In fact, one cycle of each of the figures in Fig. 5 is the horizontal projection of (the straight line and the loop) Fig. 19.

We conclude this section with a few comments. It is useful to recall that the addition of linear or quadratic dampers does not alter the passive status of the robot. We can extend the repertoire of passive elements by adding passive springs to the robot joints. Compared with natural human locomotion the passive elements may resemble the inherent damping and compliance of human joints.

The passive elements can be easily imitated by a control law in an active robot. It will be interesting to incorporate control laws based on active physical elements (negative dampers, negative springs) and see if the robot can climb uphill. A control law for the uphill walk of the robot was

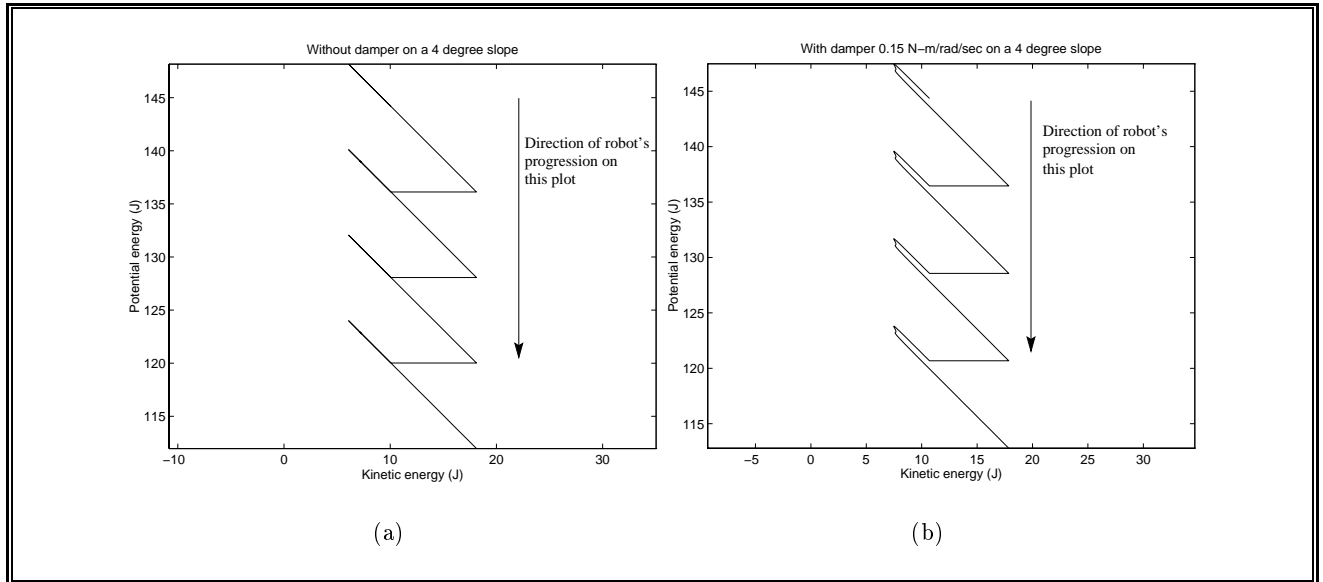


Figure 18: The KE vs PE plots during steady robot gaits on 4° slope. Fig. 18(a) represents a damper-less motion and Fig. 18(b) corresponds to motion of the robot having a 0.15 N-m/rad/sec quadratic hip damper. The swing stage dissipation of energy modifies the robot's behavior as is visible from the second plot.

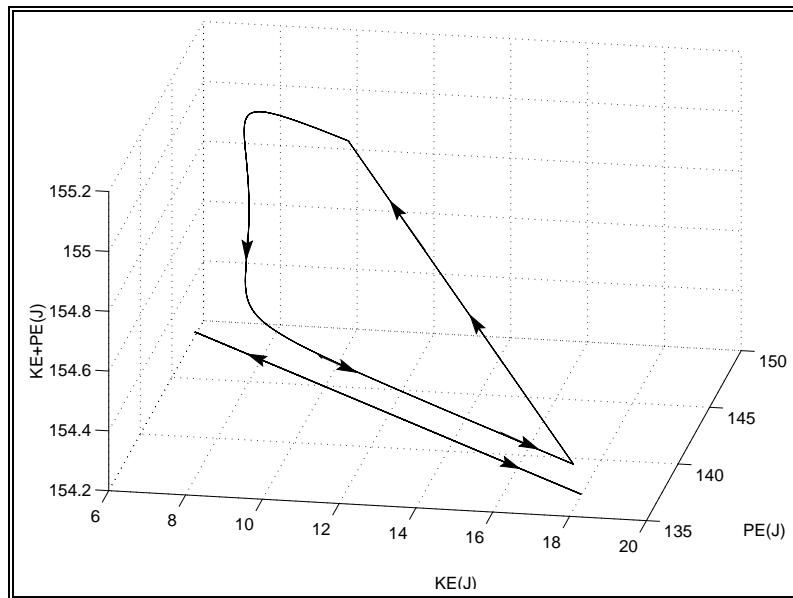


Figure 19: Here we plot the three quantities: the KE, the PE, and the total mechanical energy (KE+PE) of the robot during a steady cycle on a 4° slope. The straight line at the bottom corresponds to a damper-less robot for which KE+PE is constant. Introduction of a damper results in a continuous dissipation of system energy during motion which results in a more complicated energy diagram given by the loop. The straight line joining the extreme right hand corner of the loop to its upper portion represents the instantaneous energy absorption due to the ground impact coupled with a simultaneous shift of the coordinate frame to re-initialize PE. (needs more explanation)

presented in [11].

Our results apparently contradict the findings of [26] which reported that even a small amount of friction (by which damping was meant) in the hip joint can destroy the cycle. We have found that the original cycle is modified to another cycle rather than being destroyed.

Finally let us mention that the addition of a quadratic damper $\propto (\theta_{ns})^2$ *dramatically* influences the robot behavior. With this damper in action the robot can possess extremely large limit cycle attraction basins and can deal with steep slopes (we have found steady gaits up to 20°) which are impossible otherwise. The implications of this are not clear and the implementation of such a damper (either passively or actively) is, at least, not straightforward.

6 Conclusions and future work

We have made a systematic study of the passive gait of a planar biped robot with compass-like motion. We have shown that any of the three parameters, namely the ground slope, and the normalized mass and length of the robot, affect the robot gait in the same qualitative manner. As we gradually increase one of the parameters, the symmetric and steady stable gaits of the unpowered robot evolve through a regime of bifurcations characterized by progressively more complicated asymmetric gaits, eventually arriving at an apparently chaotic gait where no two steps are identical.

Although it could not predict the long-term behavior of the robot, the linear model helped us making guesses of the initial states of the robot that lie in the basin of attraction of a limit cycle corresponding to the slope. We found that the linear model was valid for small β and small μ . It was interesting to note that the validity of the linear solution was not a function of the third parameter, μ .

The asymptotic stability of a dynamic system must be accompanied by a reduction of the phase fluid volume and the only source of volume contraction in this idealized frictionless robot are the transition equations. We have measured the phase fluid volume contraction which quantifies the rate of convergence of nearby trajectories. A typical contraction ratio was calculated to be 0.1, showing strong contraction.

Presence of a passive damper in the hip joint (the only real joint) of the robot significantly increases gait stability and versatility. Although even a linear damper has a beneficial influence, we chose to present the results based on quadratic dampers for their better performance. With the other three parameters constant, different dampers produce different gait cycles. Note that our results apparently contradict the findings of [26] who reported that a hip damper destroys a stable limit cycle.

Before discussing the possible extensions of this work let us mention two interesting facts regarding the behavior of the robot. First, we have found that the robot can accept, without falling down, a *much* larger perturbation of the velocity states than the position states. For example, for the gait on a 3° slope, the state $\dot{\theta}_{ns}$ could absorb a perturbation of more than $100^\circ/\text{sec}$ whereas a perturbation of even 2° of the state θ_{ns} takes the states out of the attraction basin. The same phenomenon was noted by [26]. Interestingly we have noticed similar behavior for a different system with impacting elements [24] governed by hybrid equations. Is this behavior common to all systems, hybrid systems and/or those involving impacts?

A second fact is that there is a strong indication that *all* the motion descriptors of the gait of a given robot model are specified by only one parameter, the ground slope angle. This hints towards a strong underlying organizing principle.

For the future, it is possible to place passive biped robots in the larger perspective of passive machines including not only massive links but also the other passive elements such as springs and dampers. This will necessitate a systematic study of the effect of these other elements on the purely inertial dynamics of the robot. We can furnish three main reasons supporting this study. First, as we have already seen in this article, additional passive elements are very promising in significantly improving the gait stability and gait versatility. Second, we obtain a rich source of simple active control laws which may mimic the physical behavior of passive elements. Third, a better understanding of the gait itself may be obtained by analyzing the role played by the passive elements.

The transition equations play a fundamental role in the global dynamics of the robot. Our transition equations are derived from the law of conservation of angular momentum, which models the effect of ground impact on the robot. There are other ways to address the issue. One can, for example, create a physical spring-damper model of the ground and add it to the robot model. In

any case, the results will be reliable if the gait features are qualitatively preserved for small changes in the parameters of the model.

The difficulties in studying the behavior of this apparently simple biped mechanism are to a large part due to its hybrid algebro-differential governing equations. Better analytical tools for dealing with such systems are needed. In particular, an estimation, even numerical, of the size of the basin of attraction of a limit cycle would be of immense value, both from the theoretical and practical points of view.

Currently, it is difficult to extend the insights obtained with a simple robot model to even a slightly more complex one. Our final challenge lies in the judicious interpretation of the results obtained for this simple biped so that we can progress towards our objective of understanding human locomotion and extend the results to higher degrees-of-freedom robots.

References

- [1] P. Bergé, Y. Pomeau, and C. Vidal. *Order within chaos*. John Wiley & sons, 1984.
- [2] M.D. Berkemeier and R.S. Fearing. Control of a two-link robot to achieve sliding and hopping gaits. In *Proc. of IEEE Conf. on Robotics and Automation*, volume 1, pages 286–291, Nice, 1992.
- [3] D.J. Block and M.W. Spong. Mechanical design & control of the pendubot. In *SAE Earth-moving Industry Conference*, Peoria, IL, 1995.
- [4] M. Coleman and A. Ruina. A Tinkertoy^(rg. tr.) model that walks. *Physical Review Letters (submitted)*, 1997.
- [5] B. Espiau. Bip: A joint project for the development of an anthropomorphic biped robot. In *Proc. of the International Conference on Advanced Robotics*, July 1997.
- [6] B. Espiau and A. Goswami. Compass gait revisited. In *Proc. IFAC Symposium on Robot Control (SYROCO)*, pages 839–846, Capri, September 1994.
- [7] A. Formal'sky. Ballistic locomotion of a biped. Design and control of two biped machines. In A. Morecki and K. J. Waldron, editors, *Human and Machine Locomotion*, Udine, Italy, 1997. Springer Wien, New York.
- [8] C. François. *Contribution à la locomotion articulée dynamiquement stable (in French)*. PhD thesis, Ecole des Mines de Paris, April 1996.
- [9] M. Garcia, A. Chatterjee, A. Ruina, and M. Coleman. The simplest walking model: Stability, complexity, and scaling. *ASME Journal of Biomechanical Engineering (accepted)*, 1997.
- [10] A. Goswami, B. Espiau, and A. Keramane. Limit cycle and their stability in a passive bipedal gait. In *Proc. of IEEE Conf. on Robotics and Automation*, pages 246–251, Minneapolis, April 1996.
- [11] A. Goswami, B. Espiau, and A. Keramane. Limit cycles in a passive compass gait biped and passivity-mimicking control laws. *Journal of Autonomous Robots*, 4:273–286, 1997.
- [12] A. Goswami, B. Thuilot, and B. Espiau. Compass-like biped robot part I: Stability and bifurcation of passive gaits. Technical report, INRIA, No. 2996, Oct. 1996.
- [13] A.A. Grishin, A.M. Formalsky, A.V. Lensky, and S.V. Zhitomirsky. Dynamic walking of a vehicule with two telescopic legs controlled by two drives. *The International Journal of Robotics Research*, 13(2):137–147, April 1994.
- [14] J. Guckenheimer and P. Holmes. *Nonlinear Oscillations, Dynamical Systems, and Bifurcations*. Springer-Verlag, New York, 1983.
- [15] C. Hayashi. *Nonlinear Oscillations in Physical Systems*. Princeton Univ Press, NJ, 1985.
- [16] P.S. Heckbert (ed.). *Graphics Gems IV*. Academic Press, 1994.
- [17] R. C. Hilborn. *Chaos & Nonlinear Dynamics*. Oxford University Press Inc., 1994.
- [18] Y. Hurmuzlu and T.H. Chang. Rigid body collisions of a special class of planar kinematic chains. *IEEE Transactions on Systems, Man and Cybernetics*, 22(5):964–971, 1992.
- [19] Y. Hurmuzlu and G.D. Moskowitz. The role of impact in the stability of bipedal locomotion. *Dynamics and Stability of Systems*, 1(3):217–234, 1986.

- [20] Y. Hurmuzlu and G.D. Moskowitz. Bipedal locomotion stabilized by impact and switching: I and II. *Dynamics and Stability of Systems*, 2(2):73–112, 1987.
- [21] R. Katoh and M. Mori. Control method of biped locomotion giving asymptotic stability of trajectory. *Automatica*, 20(4):405–411, 1984.
- [22] D. Koditschek and M. Bühler. Analysis of a simplified hopping robot. *The International Journal of Robotics Research*, 10(6), 1991.
- [23] C. Lanczos. *The Variational Principles of Mechanics*. Dover Publications, Inc., New York, 1986.
- [24] M. Mata-Jimenez, B. Brogliato, and A. Goswami. On the control of mechanical systems with dynamic backlash. In *CDC Conference (accepted)*, San Diego, 1997.
- [25] R.T. McCloskey and J.W. Burdick. An analytical study of simpl hopping robots with vertical and forward motion. In *Proc. IEEE Robotics & Automation*, volume 2, pages 1392–1397, Sacramento, April 1991.
- [26] T. McGeer. Passive dynamic walking. *Int. J. of Rob. Res.*, 9(2):62–82, 1990.
- [27] T.A. McMahon. *Muscles, Reflexes, and Locomotion*. Princeton University Press, 1984.
- [28] S. Mochon and T.A. McMahon. Ballistic walking: an improved model. *Mathematical Bioscience*, 52:241–260, 1981.
- [29] J.P. Ostrowski and J.W. Burdick. Designing feedback algorithms for controlling the periodic motions of legged robots. In *Proc. IEEE Robotics & Automation*, volume 2, pages 260–266, Atlanta, May 1993.
- [30] T.S. Parker and L. O. Chua. *Practical numerical algorithms for chaotic systems*. Springer, Berlin, 1989.
- [31] M.H. Raibert. *Legged Robots that Balance*. MIT Press, Cambridge, USA, 1986.
- [32] J. Rose and J.G. Gamble (eds). *Human Walking*. Williams & Wilkins, Baltimore, USA, 1994.
- [33] Scilab-2.2. *INRIA* Domaine de Voluceau, Rocquencourt, France, February 1997.
- [34] M.W. Spong. The swing up control problem for the acrobot. *IEEE Control Systems Magazine*, February 1995.
- [35] B. Thuilot, A. Goswami, and B. Espiau. Bifurcation and chaos in a simple passive bipedal gait. In *Proc. of IEEE Conf. on Robotics and Automation*, pages 792–798, Albuquerque, April 1997.
- [36] H. Troger and A. Steindl. *Nonlinear stability and bifurcation theory*. Springer Verlag, Wien, 1991.
- [37] A.F. Vakakis and J.W. Burdick. Chaotic motions in the dynamics of a hopping robot. In *Proc. IEEE Robotics & Automation*, volume 3, pages 1464–1469, Cincinnati, May 1990.
- [38] J-S. Yang. A control study of a kneeless biped locomotion system. *Journal of the Franklin Institute*, 331B(2):125–143, 1994.